A multilayer method for the hydrostatic Navier-Stokes equations: a particular weak solution

E.D. Fernández-Nieto [*], E.H. Koné [†], T. Chacón Rebollo [‡]

July 30, 2013

Abstract

In this work we present a mutilayer approach to the solution of non-stationnary 3D Navier-Stokes equations. We use piecewise smooth weak solutions. We approximate the velocity by a piecewise constant (in z) horizontal velocity and a linear (in z) vertical velocity in each layer, possibly discontinuous across layer interfaces. The multilayer approach is deduced by using the variational formulation and by considering a reduced family of test functions. The procedure naturally provides the mass and momentum interfaces conditions. The mass and momentum conservation across interfaces is formulated via normal flux jump conditions. The jump conditions associated to momentum conservation are formulated by means of an approximation of the vertical derivative of the velocity that appears in the stress tensor. We approximate the multilayer model for hydrostatic pressure, by using a PVM finite volume scheme and we present some numerical tests that show the main advantages of the model: it improves the approximation of the vertical velocity, provides good predictions for viscous effects and simulates re-circulations behind solid obstacles.

[*]Corresponding author. Dpto. Matemática Aplicada I. ETS Arquitectura - Universidad de Sevilla. Avda. Reina Mercedes N. 2. 41012-Sevilla, Spain. (edofer@us.es)

[†]Dpto. Matemática Aplicada I. ETS Arquitectura - Universidad de Sevilla. Avda. Reina Mercedes N. 2. 41012-Sevilla, Spain. (ekone@us.es)

[‡]IMUS &Dpto. Ecuaciones Diferenciales y Análisis Numérico, U. Sevilla. C/ Tarfia, s/n. 41080 Sevilla, Spain and BCAM - Basque Center for Applied Mathematics, Alameda de Mazarredo, 14, 48009 Bilbao, Spain (chacon@us.es).

1 Introduction

Multilayer Saint-Venant (or shallow water) models are commonly used techniques to study hydrodynamic flows with large friction, with significant water depth and/or with important wind effects, among others (see for example [5], [8], [17]). In these cases, the standard shallow water system is considered invalid since the horizontal velocity can hardly be approximated by a vertically constant velocity in the whole domain.

The multilayer approach consists in subdividing, in the vertical direction, the domain into shallow layers in order to apply inside the classic hypothesis of Saint-Venant. In the multilayer Saint-Venant system derived by Audusse et al. in [3] the layers are assumed to be advected by the flow. Then, no mass exchange occurs between neighboring layers making the model physically closer to non-miscible fluids simulation. That model is also extended to 3D computations of free surface flows with friction and viscosity effects by Audusse et al. in [6]. A different multilayer model with a hydrostatic framework is proposed by Audusse et al. in [8]. Each layer is pre-set, described by its height and by a vertically constant horizontal velocity. The main improvement is that mass and momentum exchanges between the layers are allowed. In order to close the system, the height of the layer is related to the total height of the fluid. Then, the unknowns of the system are the total height of the fluid and a constant horizontal velocity at each layer. The vertical velocity can be computed by postprocessing, taking into account the incompressibility of the fluid. The model has been extended by Audusse et al. in [7] to variable density flows, and by Sainte-Marie in [12] to non-hydrostatic flows.

In the present work, we derive a multilayer method from a variational formulation of the unsteady incompressible free surface Navier-Stokes equations. The method that we propose in this paper can be seen as a splitting technique, where first we approximate the vertical variations of the solution of the full problem. It is obtained by approximating the solution in a vertical partition with a discontinuous profile. We consider an approximation of the horizontal velocity and of the vertical velocity that respectively are constant and linear in the vertical variable. Then, we deduce the model obtained from the standard variational formulation of Navier-Stokes equations, by supposing this discontinuous vertical profile of the solution for a reduced family of test functions. Therefore, the solution of the deduced model is an approximation of the weak solution of the full model, in the sense that it verifies the weak variational formulation of the full model for a particular family of test functions (see [1] and [2]).

In fact, the multilayer method that we propose must not be considered as a model, it is a numerical method. Where first we discretize the vertical variable by using a finite element framework with discontinous $\mathbb{P}_0$ function tests. And in a second step we discretize the horizontal variable with the method that we prefer. Then, one question is if the actual method "defined as a multilayer model" is more efficient than other numerical techniques to treat with the solution of Navier-Stokes equations with hydrostatic pressure and free surface. From a technical point of view note that the multilayer approach allows to reduce in one dimension the computational cells. Avoiding in this case the problem to treat with the free surface with 3D meshes (or 2D vertical meshes). By another way, mass conservation is ensured, by while if we discretize the Navier-Stokes equations with free surface by some finite element 3D method then mass conservation depend strongly on the way as the free surface movement is treated. It is difficult to compare exactly the computational cost of different numerical techniques, for example it depends on the efficiency of the coding process. But as the multilayer approach enables to approximate free surface flows without an extra difficulty, it can be computationally less expensive than some other numerical techniques to approach the full 3D model for free-surface flows. For instance, in [6] the authors remark that a comparable

test using 6 layers (1452 nodes, 2620 triangles for the 2D mesh) takes a CPU time of 10 minutes for the multilayer and 33 minutes for the hydrostatic Navier-Stokes solver.

Even if we start with a general framework, we finally restrict ourselves to a hydrostatic pressure framework. The non-hydrostatic case will be issued in a forthcoming paper. The model we derive allows also mass and momentum transference between the neighboring layers as the one proposed in [8]. However, here the discontinuity of the velocity and the pressure at the interfaces are related to the normal flux jump conditions associated to mass and momentum conservation. The stress tensor that appears in the momentum conservation jump conditions include the vertical derivative of the velocity, which is conveniently approximated. Moreover, the vertical velocity is drawn from the model and includes a linear vertical profile per layer.

The remainder of the paper is organized as follows. In Section 2, we present the deduction of the multilayer model. We start by stating the interfaces mass and momentum conditions which come out from the weak formulation, next we detail the procedure yielding the model for a hydrostatic pressure. In Section 4, we close the hydrostatic multilayer system and develop some computations to rewrite the model under the structure of an hyperbolic system with conservative components, nonconservative products and source terms. Then we present the finite volume procedure to resolve the model. In Section 5, we present two numerical tests. Finally, the conclusions of the paper are set in Section 6.

2 A multilayer approach

In this section we deduce a multilayer system of partial differential equations from the Navier-Stokes equations.

The multilayer system that we propose in this work can be seen as a technique to approximate the solution of the Navier-Stokes equations. It is obtained as the system of partial differential equations that is verified by particular piecewise smooth weak solutions. Concretely, first we consider a vertical partition of the domain and we suppose that the solution can be approximated by a piecewise smooth function whose horizontal velocity does not depend on z at each layer. The multilayer system is deduced as the one verified by particular weak solutions in the following sense. We consider the system obtained by using smooth vector test functions which have horizontal components independent of the variable z and vertical components linear in z.

Let us consider the non-stationary free surface Navier-Stokes equations in a d-dimensional space ($d = 2, 3$). For a given positive constant real number T and each time $t \in]0, T]$, we denote by $\Omega_F(t)$, the fluid domain and by $I_F(t)$, its projection onto the horizontal plane. For given constant dynamic viscosity $\mu \in \mathbb{R}$ and gravity acceleration $g \in \mathbb{R}$, the density $\rho \in \mathbb{R}$, the pressure $p \in \mathbb{R}$ and the velocity $\underline{\underline{\vec{\boldsymbol{u}}}} := (\underline{\underline{\vec{\boldsymbol{u}}}}_H, \underline{\underline{w}})^{'} \in \mathbb{R}^d$ functions with $\underline{\underline{\vec{\boldsymbol{u}}}}_H \in \mathbb{R}^{d-1}$ satisfy the conservative system:

$$\begin{cases} \partial_t \rho \ + \ \nabla \cdot (\rho \underline{\underline{\vec{\boldsymbol{u}}}}) \ = \ 0, \\ \\ \partial_t (\rho \underline{\underline{\vec{\boldsymbol{u}}}}) \ + \ \nabla \cdot (\rho \underline{\underline{\vec{\boldsymbol{u}}}} \otimes \underline{\underline{\vec{\boldsymbol{u}}}}) \ - \ \nabla \cdot \boldsymbol{\Sigma}_T \ = \ \rho \vec{\boldsymbol{g}}, \end{cases} \tag{1}$$

where $\vec{\boldsymbol{g}} = (\boldsymbol{0}, -g)^{'} \in \mathbb{R}^d$ and the total stress tensor is $\boldsymbol{\Sigma}_T = -p\boldsymbol{I} + \mu \left(\nabla \underline{\underline{\vec{\boldsymbol{u}}}} + (\nabla \underline{\underline{\vec{\boldsymbol{u}}}})^{'} \right)$. The symbol $\boldsymbol{I}$ stands for the identity tensor. The generic space variable is $(x, z) \in \mathbb{R}^d$

such that the horizontal variable corresponds to $x = (x_1, ..., x_{d-1}) \in \mathbb{R}^{d-1}$.

In this work we will consider a flow of an incompressible fluid with a homogeneous mass density. That is, the density function $\rho(t, x, z)$ is a constant real value ρ. Nevertheless, for the sake of clarity in the exposition we retain the density dependence in the equations.

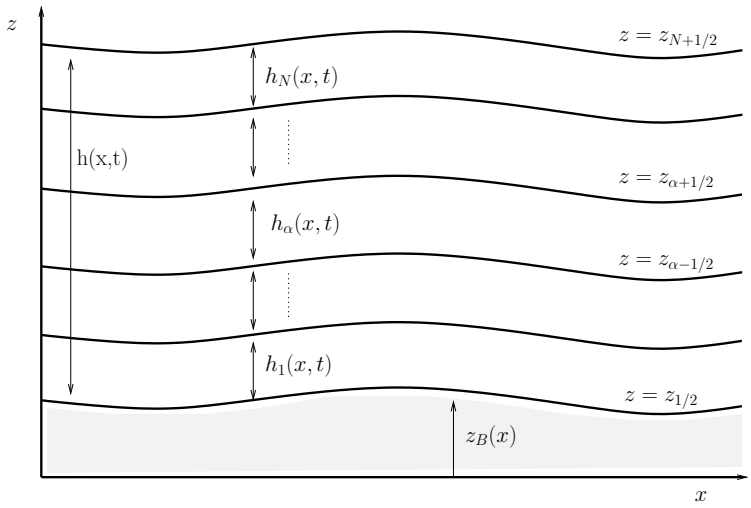

Figure 1: *Sketch of the multilayer division of the fluid domain.*

In order to introduce a multilayer system, the fluid domain is divided along the vertical direction into $N \in \mathbb{N}^*$ pre-set layers of thickness $h_\alpha(t, x)$ with $N+1$ interfaces $\Gamma_{\alpha+\frac{1}{2}}(t)$ of equations $z = z_{\alpha+\frac{1}{2}}(t, x)$ for $\alpha = 0, 1, ..., N$ and $x \in I_F(t)$ (see Figure 1). We assume that the interfaces $\Gamma_{\alpha+\frac{1}{2}}(t)$ are smooth, concretely at least of class $\mathcal{C}^1$ in time and space. We shall denote by $z_B = z_{\frac{1}{2}}$ and $z_S = z_{N+\frac{1}{2}}$ the equations of the bottom and the free surface interfaces $\Gamma_B(t)$ and $\Gamma_S(t)$, respectively. We have $h_\alpha = z_{\alpha+\frac{1}{2}} - z_{\alpha-\frac{1}{2}}$ and $z_{\alpha+\frac{1}{2}} = z_B + \sum_{\beta=1}^{\alpha} h_\beta$ for $\alpha = 1, ..., N$. Then the height of the fluid is given by $h = z_S - z_B = \sum_{\alpha=1}^{N} h_\alpha$.

Actually we have $\partial\Omega(t) = \Gamma_B(t) \cup \Gamma_S(t) \cup \Theta(t)$, where $\Theta(t)$ is the inflow/outflow boundary which we assume here to be vertical. The fluid domain is split as $\overline{\Omega_F(t)} = \cup_{\alpha=1}^{N} \overline{\Omega_\alpha(t)}$ with the setting

$$\begin{aligned}
&\Omega_\alpha(t) = \Big\{(x,z);\ x \in I_F(t) \text{ and } z_{\alpha-\frac{1}{2}} < z < z_{\alpha+\frac{1}{2}}\Big\},\\
&\partial\Omega_\alpha(t) = \Gamma_{\alpha-\frac{1}{2}}(t) \cup \Gamma_{\alpha+\frac{1}{2}}(t) \cup \Theta_\alpha(t), \text{ with}\\
&\Theta_\alpha(t) = \Big\{(x,z);\ x \in \partial I_F(t) \text{ and } z_{\alpha-\frac{1}{2}} < z < z_{\alpha+\frac{1}{2}}\Big\}.
\end{aligned} \tag{2}$$

Hence the inflow/outflow boundary is split as $\overline{\Theta(t)} = \cup_{\alpha=1}^{N} \overline{\Theta_\alpha(t)}$.

Moreover, let us introduce the following notation:

(i) For two tensors $\boldsymbol{a}$ and $\boldsymbol{b}$ of sizes (n, m) and (n, p) respectively, we shall denote by $(\boldsymbol{a};\ \boldsymbol{b})$ the tensor of size $(n, m+p)$ which is the concatenation of $\boldsymbol{a}$ and $\boldsymbol{b}$ in this order.

(ii) Let the differential operator $\nabla = (\partial_{x_1}, ..., \partial_{x_{d-1}}, \partial_z)$, Then we set $\overline{\nabla} := (\partial_t;\ \nabla) = (\partial_t, \partial_{x_1}, ..., \partial_{x_{d-1}}, \partial_z)$ and $\nabla_x := (\partial_{x_1}, ..., \partial_{x_{d-1}})$.

(iii) For $\alpha = 0, 1, ..., N$ and for a function f, we set

$$f^-_{\alpha+\frac{1}{2}} := (f_{|\Omega_\alpha(t)})_{|\Gamma_{\alpha+\frac{1}{2}}(t)} \text{ and } f^+_{\alpha+\frac{1}{2}} := (f_{|\Omega_{\alpha+1}(t)})_{|\Gamma_{\alpha+\frac{1}{2}}(t)}.$$

When the function f is continuous, we will merely set

$$f_{\alpha+\frac{1}{2}} := f_{|\Gamma_{\alpha+\frac{1}{2}}(t)}.$$

(iv) We will denote by $\vec{\boldsymbol{\eta}}_{\alpha+\frac{1}{2}}$ the space unit normal vector to the interface $\Gamma_\alpha(t)$ outward to the layer $\Omega_\alpha(t)$ for a given time t for $\alpha = 0, ..., N$. It is defined by

$$\vec{\boldsymbol{\eta}}_{\alpha+1/2} = \frac{\left(\nabla_x z_{\alpha+\frac{1}{2}}, -1\right)'}{\sqrt{1 + \left|\nabla_x z_{\alpha+\frac{1}{2}}\right|^2}}. \tag{3}$$

(v) We will denote by $\vec{\boldsymbol{n}}_{T,\alpha+\frac{1}{2}}$ the (space-time) unit normal vector to the interface $\Gamma_\alpha(t)$ outward to the layer $\Omega_\alpha(t)$ for $\alpha = 0, ..., N$,

$$\vec{\boldsymbol{n}}_{T,\alpha+1/2} = \frac{\left(\partial_t z_{\alpha+\frac{1}{2}}, \nabla_x z_{\alpha+\frac{1}{2}}, -1\right)'}{\sqrt{1 + \left|\nabla_x z_{\alpha+\frac{1}{2}}\right|^2 + (\partial_t z_{\alpha-\frac{1}{2}})^2}}.$$

Remark 1 *Adding the time variable as one more dimension, the corresponding domain Ω_T is actually given by*

$$\begin{aligned}
&\Omega_T = \Big\{(t,x,z);\ t \in]0,T] \text{ and } (x,z) \in \Omega_F(t)\Big\}, \text{ with}\\
&\partial\Omega_T = \Lambda_T \cup \Lambda_1 \cup \Lambda_2, \text{ where}\\
&\Lambda_T = \Big\{(t,x,z);\ t \in]0,T] \text{ and } (x,z) \in \partial\Omega_F(t)\Big\},\\
&\Lambda_1 = \Big\{(0,x,z);\ (x,z) \in \Omega_F(0)\Big\},\\
&\Lambda_2 = \Big\{(T,x,z);\ (x,z) \in \Omega_F(T)\Big\}.
\end{aligned}$$

Since we integrate over $\Omega_F(t)$, we retain here the boundary Λ_T for the computations even if it means cancelling the tests functions over the boundaries Λ_1 and Λ_2.

2.1 Weak solution with discontinuities

Let us recall the conditions to be verified by a piecewise smooth weak solution $(\underline{\vec{\boldsymbol{u}}}, p, \rho)$ of (1). More precisely, let us suppose that the velocity $\underline{\vec{\boldsymbol{u}}}$, the pressure p and the density ρ are smooth in each $\Omega_\alpha(t)$, but possibly discontinuous across the predetermined hypersurfaces $\Gamma_{\alpha+\frac{1}{2}}(t)$ for $\alpha = 1, ..., N-1$. Then the triplet $(\underline{\vec{\boldsymbol{u}}}, p, \rho)$ is a weak solution of (1) if the following conditions hold:

(i) $(\underline{\vec{\boldsymbol{u}}}, p, \rho)$ is a standard weak solution of (1) in each layer $\Omega_\alpha(t)$.

(ii) $(\underline{\vec{\boldsymbol{u}}}, p, \rho)$ satisfies the normal flux jump conditions at $\Gamma_{\alpha+\frac{1}{2}}(t)$, for $\alpha = 0, \dots, N$:

- For the mass conservation law,

$$[(\rho;\ \rho\underline{\vec{\boldsymbol{u}}})]_{|_{\Gamma_{\alpha+\frac{1}{2}}(t)}} \cdot \quad \vec{\boldsymbol{n}}_{T,\alpha+1/2} = 0, \tag{4}$$

- For the momentum conservation law,

$$\Big[(\rho\underline{\vec{\boldsymbol{u}}};\ \rho\underline{\vec{\boldsymbol{u}}} \otimes \underline{\vec{\boldsymbol{u}}} - \boldsymbol{\Sigma}_T)\Big]_{|_{\Gamma_{\alpha+\frac{1}{2}}(t)}} \cdot \quad \vec{\boldsymbol{n}}_{T,\alpha+1/2} = 0, \tag{5}$$

where $[(a;\ b)]_{|_{\Gamma_{\alpha+\frac{1}{2}}(t)}}$ denotes the the jump of the pair $(a;\ b)$ across $\Gamma_{\alpha+\frac{1}{2}}(t)$,

$$[(a;\ b)]_{|_{\Gamma_{\alpha+\frac{1}{2}}(t)}} = \Big((a;\ b)_{|_{\Omega_{\alpha+1}(t)}} - (a;\ b)_{|_{\Omega_\alpha(t)}}\Big)_{|_{\Gamma_{\alpha+\frac{1}{2}}(t)}}$$

In order to develop the multilayer model, we adapt the preceding conditions to a particular class of pairs velocity-pressure: We assume the layers thicknesses small enough to neglect the dependence of the horizontal velocities and the pressure on the vertical variable inside each layer. Moreover, we assume that the vertical velocity is piecewise linear in z, and possibly discontinuous. Concretely, we set

$$\vec{\boldsymbol{u}}_{|_{\Omega_\alpha(t)}} := \vec{\boldsymbol{u}}_\alpha := (\vec{\boldsymbol{u}}_{H,\alpha}, w_\alpha)', \quad p_\alpha := p_{|_{\Omega_\alpha(t)}},$$

where $\vec{\boldsymbol{u}}_{H,\alpha}$ and w_α respectively stand for the horizontal and vertical velocities on layer α, and assume

$$\partial_z \vec{\boldsymbol{u}}_{H,\alpha} = 0, \quad \partial_z p_\alpha = 0, \quad \partial_z w_\alpha = d_\alpha(t,x), \tag{6}$$

for some smooth function $d_\alpha(t,x)$. In addition, in the present work we shall consider globally constant (and known) density.

There is no hope for such a particular triplet $\Big((\vec{\boldsymbol{u}}_{H,\alpha}, w_\alpha)', p_\alpha\Big)$ to be a solution of the complete Navier-Stokes equations in the layer $\Omega_\alpha(t)$. Instead, we shall consider a reduced weak formulation with particular test functions, that we describe in Section 3.

Concerning the jump conditions, those that come from the hyperbolic part of Navier-Stokes equations may exactly be set for our approximated solution. However, the elliptic part involves vertical derivatives that need a further approximation. We proceed as follows:

2.1.1 Mass conservation jump conditions

Observe that

$$\vec{\boldsymbol{u}}^+_{H,\alpha-\frac{1}{2}}(t,x) \ = \ \vec{\boldsymbol{u}}^-_{H,\alpha+\frac{1}{2}}(t,x) \ = \ \vec{\boldsymbol{u}}_{H,\alpha}(t,x). \tag{7}$$

Then $\vec{\boldsymbol{u}}$ satisfies the mass conservation jump conditions if

$$G_{\alpha+\frac{1}{2}} := G^-_{\alpha+\frac{1}{2}} = G^+_{\alpha+\frac{1}{2}}, \tag{8}$$

where

$$\begin{cases} G^+_{\alpha+\frac{1}{2}} = \partial_t z_{\alpha+\frac{1}{2}} + \vec{\boldsymbol{u}}_{H,\alpha+1} \cdot \nabla_x z_{\alpha+\frac{1}{2}} - w^+_{\alpha+\frac{1}{2}}, \\ G^-_{\alpha+\frac{1}{2}} = \partial_t z_{\alpha+\frac{1}{2}} + \vec{\boldsymbol{u}}_{H,\alpha} \cdot \nabla_x z_{\alpha+\frac{1}{2}} - w^-_{\alpha+\frac{1}{2}}. \end{cases}$$

Observe that $G_{\alpha+\frac{1}{2}}$ is the normal mass flux at the interface $\Gamma_{\alpha+\frac{1}{2}}(t)$.

2.1.2 Momentum conservation jump conditions

Using (8) condition (5) can be written in terms of the normal mass flux. Indeed, (5) can also be written as

$$\Big[\boldsymbol{\Sigma}\Big]_{|\Gamma_{\alpha+\frac{1}{2}}(t)} \cdot \Big(\nabla_x z_{\alpha+\frac{1}{2}}, -1\Big) = \Big[(\rho\underline{\vec{\boldsymbol{u}}};\ \rho\underline{\vec{\boldsymbol{u}}} \otimes \underline{\vec{\boldsymbol{u}}})\Big]_{|\Gamma_{\alpha+\frac{1}{2}}(t)} \cdot \Big(\partial_t z_{\alpha+\frac{1}{2}}, \nabla_x z_{\alpha+\frac{1}{2}}, -1\Big).$$

Also, by (8),

$$\Big[(\rho\underline{\vec{\boldsymbol{u}}};\ \rho\underline{\vec{\boldsymbol{u}}} \otimes \underline{\vec{\boldsymbol{u}}})\Big]_{|\Gamma_{\alpha+\frac{1}{2}}(t)} \cdot \Big(\partial_t z_{\alpha+\frac{1}{2}}, \nabla_x z_{\alpha+\frac{1}{2}}, -1\Big) = \rho\, G_{\alpha+\frac{1}{2}}\ [\vec{\boldsymbol{u}}]_{|\Gamma_{\alpha+\frac{1}{2}}(t)}.$$

We deduce that condition (5) can be written as

$$\Big[\boldsymbol{\Sigma}\Big]_{|\Gamma_{\alpha+\frac{1}{2}}(t)} \cdot \vec{\boldsymbol{\eta}}_{\alpha+\frac{1}{2}} = \frac{\rho\, G_{\alpha+\frac{1}{2}}}{\sqrt{1+\Big|\nabla_x z_{\alpha+\frac{1}{2}}\Big|^2}}\ [\vec{\boldsymbol{u}}]_{|\Gamma_{\alpha+\frac{1}{2}}(t)}. \tag{9}$$

Remark 2 *The momentum interfaces conditions* (9) *naturally points out that there is no jump in the stress at the interface* $\Gamma_{\alpha+\frac{1}{2}}(t)$ *when either the velocity is continuous or there is no mass transference between the layers (i.e.* $G_{\alpha+\frac{1}{2}} = 0$*), that occurs when* $\Gamma_{\alpha+\frac{1}{2}}(t)$ *is a material surface.*

As we consider a vertical discontinuous profile, to approximate the second order derivatives in z, we use a mixed formulation (see for example [19]). We introduce an additional auxiliary unknown $\vec{\mathbf{Q}}$ that satisfies the equation

$$\vec{\mathbf{Q}} - \partial_z \vec{\boldsymbol{u}} = 0, \quad \text{with} \quad \vec{\mathbf{Q}} = (\vec{\mathbf{Q}}_H, Q_v). \tag{10}$$

And to approximate $\vec{\mathbf{Q}}$, solution of (10), we approximate $\vec{\boldsymbol{u}}$ by $\widetilde{\vec{\boldsymbol{u}}}$, a $\mathbb{P}_1(z)$ interpolation such that $\widetilde{\vec{\boldsymbol{u}}}_{|z=\frac{1}{2}(z_{\alpha-\frac{1}{2}}+z_{\alpha+\frac{1}{2}})} = \vec{\boldsymbol{u}}_\alpha$.

For $\alpha = 1, ..., N-1$, the total stress writes

$$\boldsymbol{\Sigma}^\pm_{\alpha+\frac{1}{2}} = -p_{\alpha+\frac{1}{2}}\, \boldsymbol{I} + \mu\, D^\pm_{\alpha+\frac{1}{2}}, \tag{11}$$

where $p_{\alpha+\frac{1}{2}}$ is the kinematic pressure and $D^\pm_{\alpha+\frac{1}{2}}$ are approximations of $D(\vec{\boldsymbol{u}}) = \nabla\vec{\boldsymbol{u}} + (\nabla\vec{\boldsymbol{u}})'$ at $\Gamma_{\alpha+\frac{1}{2}}$. By the jump condition $D^\pm_{\alpha+\frac{1}{2}}$ must verify

$$\mu\Big(D^+_{\alpha+\frac{1}{2}} - D^-_{\alpha+\frac{1}{2}}\Big) \cdot \vec{\boldsymbol{\eta}}_{\alpha+\frac{1}{2}} = \frac{G_{\alpha+\frac{1}{2}}}{\sqrt{1+\Big|\nabla_x z_{\alpha+\frac{1}{2}}\Big|^2}} \Big[\vec{\boldsymbol{u}}\Big]_{|\Gamma_{\alpha+\frac{1}{2}}(t)}, \tag{12}$$

and by consistency, $D^{\pm}_{\alpha+\frac{1}{2}}$ must verify

$$\frac{1}{2}\Big(D^{+}_{\alpha+\frac{1}{2}} + D^{-}_{\alpha+\frac{1}{2}}\Big) = \widetilde{D}_{\alpha+\frac{1}{2}}, \tag{13}$$

where $\widetilde{D}_{\alpha+\frac{1}{2}}$ is an approximation of $D(\vec{\boldsymbol{u}})_{|\Gamma_{\alpha+\frac{1}{2}}}$. Concretely, we set

$$\widetilde{D}_{\alpha+\frac{1}{2}} = \begin{pmatrix} D_H\left(\dfrac{\vec{\boldsymbol{u}}^{+}_{H,\alpha+\frac{1}{2}} + \vec{\boldsymbol{u}}^{-}_{H,\alpha+\frac{1}{2}}}{2}\right) & \left(\nabla_x\left(\dfrac{w^{+}_{\alpha+\frac{1}{2}} + w^{-}_{\alpha+\frac{1}{2}}}{2}\right)\right)' + \vec{\mathbf{Q}}_{H,\alpha+\frac{1}{2}} \\ \nabla_x\left(\dfrac{w^{+}_{\alpha+\frac{1}{2}} + w^{-}_{\alpha+\frac{1}{2}}}{2}\right) + (\vec{\mathbf{Q}}_{H,\alpha+\frac{1}{2}})' & 2\,Q_{v,\alpha+\frac{1}{2}} \end{pmatrix}, \tag{14}$$

where $\vec{\mathbf{Q}}_{\alpha+\frac{1}{2}} = \vec{\mathbf{Q}}(\widetilde{\vec{\boldsymbol{u}}})$ at $\Gamma_{\alpha+\frac{1}{2}}$.

Finally, we can solve the system defined by (12) and the equation resulting to multiply scalarly (13) by vector $\vec{\boldsymbol{\eta}}_{\alpha+\frac{1}{2}}$. This way, we obtain the expression of $D^{\pm}_{\alpha+\frac{1}{2}}$, that verify the jump condition and the consistency condition on the interface. We can solve it easily and we obtain

$$\mu\, D^{\pm}_{\alpha+\frac{1}{2}} \cdot \vec{\boldsymbol{\eta}}_{\alpha+\frac{1}{2}} = \quad \mu \widetilde{D}_{\alpha+\frac{1}{2}} \cdot \vec{\boldsymbol{\eta}}_{\alpha+\frac{1}{2}} \pm \frac{1}{2} \frac{G_{\alpha+\frac{1}{2}}}{\sqrt{1 + \left|\nabla_x z_{\alpha+\frac{1}{2}}\right|^2}}\, [\vec{\boldsymbol{u}}]_{|\Gamma_{\alpha+\frac{1}{2}}(t)} \cdot \tag{15}$$

Let us denote by $\{\vec{\boldsymbol{\tau}}_{i,\alpha+\frac{1}{2}}\}_{i=1,2}$ an orthogonal basis of the tangent space to $\Gamma_{\alpha+\frac{1}{2}}(t)$. Let us consider the following decomposition of the stress tensor, for $\alpha = 1, ..., N-1$,

$$\boldsymbol{\Sigma}^{\pm}_{T,\alpha+\frac{1}{2}} \cdot \vec{\boldsymbol{\eta}}_{\alpha+\frac{1}{2}} = -\widetilde{p^{\pm}_{\alpha+\frac{1}{2}}} \vec{\boldsymbol{\eta}}_{\alpha+\frac{1}{2}} + \sum_{i=1}^{2} c^{\pm}_{i,\alpha+\frac{1}{2}} \vec{\boldsymbol{\tau}}_{i,\alpha+\frac{1}{2}}, \tag{16}$$

where $\widetilde{p^{\pm}_{\alpha+\frac{1}{2}}}$ is the normal projection, corresponding to the dynamic pressure whereas $c^{\pm}_{i,\alpha+\frac{1}{2}}$ stands for the tangential projections at the interface $\Gamma_{\alpha+\frac{1}{2}}(t)$. Remark that the mass interface condition (8) implies

$$w^{+}_{\alpha+\frac{1}{2}} - w^{-}_{\alpha+\frac{1}{2}} = (\vec{\boldsymbol{u}}^{+}_{H,\alpha+\frac{1}{2}} - \vec{\boldsymbol{u}}^{-}_{H,\alpha+\frac{1}{2}}) \cdot \nabla_x z_{\alpha+\frac{1}{2}}. \tag{17}$$

Using (3), we have that

$$\vec{\boldsymbol{\eta}}_{\alpha+\frac{1}{2}} \cdot [\vec{\boldsymbol{u}}]_{|\Gamma_{\alpha+\frac{1}{2}}(t)} = 0. \tag{18}$$

That is, the velocity jump $[\vec{\boldsymbol{u}}]_{|\Gamma_{\alpha+\frac{1}{2}}(t)}$ is tangent to the interface $\Gamma_{\alpha+\frac{1}{2}}(t)$. We assume that (9) still is verified by the approximated stress tensor given by (9). Multilplying scalarly (9) by $\vec{\boldsymbol{\eta}}_{\alpha+\frac{1}{2}}$, and using (18) we obtain

$$\left(\Big[\boldsymbol{\Sigma}_T\Big]_{|\Gamma_{\alpha+\frac{1}{2}}(t)} \cdot \vec{\boldsymbol{\eta}}_{\alpha+\frac{1}{2}}\right) \cdot \vec{\boldsymbol{\eta}}_{\alpha+\frac{1}{2}} = 0.$$

Then, from (16) we obtain the usual continuity of the normal projection of the stress tensor: $\widetilde{p^+_{\alpha+\frac{1}{2}}} = \widetilde{p^-_{\alpha+\frac{1}{2}}}$, that is,

$$\widetilde{p_{\alpha+\frac{1}{2}}} := \widetilde{p^+_{\alpha+\frac{1}{2}}} = \widetilde{p^-_{\alpha+\frac{1}{2}}},$$

the dynamic pressure at the interface $\Gamma_{\alpha+\frac{1}{2}}(t)$. Moreover, from (15), by taking into account that $\vec{\boldsymbol{\eta}}_{\alpha+\frac{1}{2}}$ is orthogonal to $[\vec{\boldsymbol{u}}]_{|_{\Gamma_{\alpha+\frac{1}{2}}(t)}}$ we deduce

$$\widetilde{p_{\alpha+\frac{1}{2}}} = p_{\alpha+\frac{1}{2}} + \left(\mu \widetilde{D}_{\alpha+\frac{1}{2}} \cdot \vec{\boldsymbol{\eta}}_{\alpha+\frac{1}{2}}\right) \cdot \vec{\boldsymbol{\eta}}_{\alpha+\frac{1}{2}}. \tag{19}$$

Moreover, assuming that $\vec{\boldsymbol{\tau}}_{1,\alpha+\frac{1}{2}}$ is parallel to the velocity jump $[\vec{\boldsymbol{u}}]_{|_{\Gamma_{\alpha+\frac{1}{2}}(t)}}$ and that $\vec{\boldsymbol{\tau}}_{2,\alpha+\frac{1}{2}}$ is orthogonal to it, we deduce

$$c^{\pm}_{1,\alpha+\frac{1}{2}} = \left(\mu \widetilde{D}_{\alpha+\frac{1}{2}} \cdot \vec{\boldsymbol{\eta}}_{\alpha+\frac{1}{2}}\right) \cdot \vec{\boldsymbol{\tau}}_{1,\alpha+\frac{1}{2}} \pm \frac{1}{2} \frac{G_{\alpha+\frac{1}{2}}}{\sqrt{1+\left|\nabla_x z_{\alpha+\frac{1}{2}}\right|^2}} \left| [\vec{\boldsymbol{u}}]_{|_{\Gamma_{\alpha+\frac{1}{2}}(t)}} \right|.$$

and

$$c^{\pm}_{2,\alpha+\frac{1}{2}} = \left(\mu \widetilde{D}_{\alpha+\frac{1}{2}} \cdot \vec{\boldsymbol{\eta}}_{\alpha+\frac{1}{2}}\right) \cdot \vec{\boldsymbol{\tau}}_{2,\alpha+\frac{1}{2}}.$$

That is, the term $G_{\alpha+\frac{1}{2}}\,[\vec{\boldsymbol{u}}]_{|_{\Gamma_{\alpha+\frac{1}{2}}(t)}}$ in (15) implies that there is a discontinuity in the tangential projection of the stress tensor ($\boldsymbol{\Sigma}^{\pm}_{T,\alpha+\frac{1}{2}} \cdot \vec{\boldsymbol{\eta}}_{\alpha+\frac{1}{2}}$) in the direction of the velocity jump (i.e. $c^-_{1,\alpha+\frac{1}{2}} \neq c^+_{1,\alpha+\frac{1}{2}}$). However, the normal projection remains continuous.

2.2 Vertical velocity

Let us notice that, requiring the horizontal velocities to be independent of z, naturally sets a vertically linear profile for the vertical velocity in each layer. More precisely, as $\vec{\boldsymbol{u}}_\alpha$ is a classic solution of the equations (1) in $\Omega_\alpha(t)$, for $z \in]z_{\alpha-\frac{1}{2}}, z_{\alpha+\frac{1}{2}}[$, the vertical integration of the incompressibility equation leads to the equality

$$w_\alpha(t,x,z) \;=\; w^+_{\alpha-\frac{1}{2}}(t,x) \;-\; (z - z_{\alpha-\frac{1}{2}}) \nabla_x \cdot \vec{\boldsymbol{u}}_{H,\alpha}(t,x), \quad \text{for } \alpha = 1, ..., N.$$

In addition, from the conditions (8) at the interfaces, we express the quantities

$$w^+_{\alpha+\frac{1}{2}} \;=\; (\vec{\boldsymbol{u}}_{H,\alpha+1} - \vec{\boldsymbol{u}}_{H,\alpha}) \cdot \nabla_x z_{\alpha+\frac{1}{2}} \;+\; w^-_{\alpha+\frac{1}{2}}. \tag{20}$$

Using the horizontal velocities drawn from the model, the vertical velocities in the layers are computed using the following algorithm:

- The quantity $w^+_{\frac{1}{2}}$ is determined, from the given mass transference $G_{\frac{1}{2}}$, through the condition (8) at the bottom by

$$w^+_{\frac{1}{2}} = \vec{\boldsymbol{u}}_{H,1} \cdot \nabla_x z_B + \partial_t z_B - G_{\frac{1}{2}}.$$

- Then, for $\alpha = 1, ..., N$ and $z \in]z_{\alpha-\frac{1}{2}}, z_{\alpha+\frac{1}{2}}[$, we set

$$\begin{cases} w_\alpha(t,x,z) \;=\; w^+_{\alpha-\frac{1}{2}}(t,x) \;-\; (z - z_{\alpha-\frac{1}{2}})\nabla_x \cdot \vec{\boldsymbol{u}}_{H,\alpha}(t,x), \\ \\ w^+_{\alpha+\frac{1}{2}} \;=\; (\vec{\boldsymbol{u}}_{H,\alpha+1} - \vec{\boldsymbol{u}}_{H,\alpha}) \cdot \nabla_x z_{\alpha+\frac{1}{2}} \;+\; w^-_{\alpha+\frac{1}{2}}. \end{cases} \tag{21}$$

where

$$w^-_{\alpha+\frac{1}{2}} = w_{\alpha|_{\Gamma_{\alpha+1/2}(t)}} = w^+_{\alpha-\frac{1}{2}} - h_\alpha \nabla_x \cdot \vec{\boldsymbol{u}}_{H,\alpha}.$$

Then, the velocity vector $\vec{\boldsymbol{u}}$ is a piecewise smooth function, where $\vec{\boldsymbol{u}}(t,x,z)|_{\Omega_\alpha(t)} = \vec{\boldsymbol{u}}_\alpha(t,x,z)$ for $\alpha = 1, ..., N$ with

$$\vec{\boldsymbol{u}}_\alpha(t,x,z) = \left(\vec{\boldsymbol{u}}_{H,\alpha}(t,x),\; w^+_{\alpha-\frac{1}{2}}(t,x) \;-\; (z - z_{\alpha-\frac{1}{2}})\nabla_x \cdot \vec{\boldsymbol{u}}_{H,\alpha}(t,x) \right)', \tag{22}$$

where $w^+_{\alpha-\frac{1}{2}}(t,x)$ is computed using (21). Then, it is noteworthy that the layers depths, the horizontal velocities and the pressure are the only unknowns of the system.

Moreover, observe that condition (20) in general cannot be verified if the vertical velocity is continuous across the layers interfaces.

3 A particular weak solution with hydrostatic pressure

In this Section we finish the construtcion of the model under the hypothesis of hydrostatic pressure. This means that

$$p_\alpha(t,x,z) = p_{\alpha+\frac{1}{2}}(t,x) \;+\; \rho g(z_{\alpha+\frac{1}{2}} - z), \tag{23}$$

with

$$p_{\alpha+\frac{1}{2}}(t,x) = p_S(t,x) + \rho g \sum_{\beta=\alpha+1}^{N} h_\beta(t,x). \tag{24}$$

Here, the component $p_{\alpha+\frac{1}{2}}$ is the kinematic pressure at $\Gamma_{\alpha+\frac{1}{2}}(t)$, that appears in (19), and p_S denotes the free surface pressure. Then, the unknowns of the systems are the layer depths and the horizontal velocities.

As $\vec{\boldsymbol{u}}_\alpha$ is a weak solution of the equations (1) in $\Omega_\alpha(t)$, let us begin by considering the weak formulation of (1) in $\Omega_\alpha(t)$ for $\alpha = 1, ..., N$. Assuming $\vec{\boldsymbol{u}}_\alpha \in L^2(0,T; H^1(\Omega_\alpha(t))^3)$, $\partial_t \vec{\boldsymbol{u}}_\alpha \in L^2(0,T; L^2(\Omega_\alpha(t))^3)$ and $p_\alpha \in L^2(0,T; L^2(\Omega_\alpha(t)))$, a weak solution of Navier-Stokes equations in $\Omega_\alpha(t)$ should verify

$$
\left\{
\begin{aligned}
0 = & \int_{\Omega_\alpha(t)} (\nabla \cdot \vec{\boldsymbol{u}}_\alpha)\, \varphi \, d\Omega \\
\int_{\Omega_\alpha(t)} \rho \vec{\boldsymbol{g}} \cdot \vec{\boldsymbol{v}} \, d\Omega = & \int_{\Omega_\alpha(t)} \rho \partial_t \vec{\boldsymbol{u}}_\alpha \cdot \vec{\boldsymbol{v}} \, d\Omega + \int_{\Omega_\alpha(t)} \rho \Big(\vec{\boldsymbol{u}}_\alpha \cdot \nabla \vec{\boldsymbol{u}}_\alpha \Big) \cdot \vec{\boldsymbol{v}} \, d\Omega \\
& + \int_{\Omega_\alpha(t)} \mu \Big(\nabla \vec{\boldsymbol{u}}_\alpha + (\nabla \vec{\boldsymbol{u}}_\alpha)' \Big) : \nabla \vec{\boldsymbol{v}} \, d\Omega - \int_{\Omega_\alpha(t)} p_\alpha \nabla \cdot \vec{\boldsymbol{v}} \, d\Omega \\
& + \int_{\Gamma_{\alpha+\frac{1}{2}}(t)} \left(\left(\boldsymbol{\Sigma}^-_{T,\alpha+\frac{1}{2}} + p_{\alpha+\frac{1}{2}} \boldsymbol{I} \right) \cdot \vec{\boldsymbol{\eta}}_{\alpha+\frac{1}{2}} \right) \cdot \vec{\boldsymbol{v}} \, d\Gamma \\
& - \int_{\Gamma_{\alpha-\frac{1}{2}}(t)} \left(\left(\boldsymbol{\Sigma}^+_{T,\alpha-\frac{1}{2}} + p_{\alpha-\frac{1}{2}} \boldsymbol{I} \right) \cdot \vec{\boldsymbol{\eta}}_{\alpha-\frac{1}{2}} \right) \cdot \vec{\boldsymbol{v}} \, d\Gamma,
\end{aligned}
\right. \tag{25}
$$

for all $\varphi \in L^2(\Omega_\alpha(t))$ and for all $\vec{\boldsymbol{v}} \in H^1(\Omega_\alpha(t))^3$.

We consider velocity-pressure pairs with the structure given by (6), that satisfy the previous system with particular weak solutions that verify (25) for test functions such that $\partial_z \varphi = 0$ and

$$
\vec{\boldsymbol{v}}(t,x,z) = \Big(\vec{\boldsymbol{v}}_H(t,x),\ (z - z_B)\, V(t,x) \Big)'. \tag{26}
$$

where $\vec{\boldsymbol{v}}_H$ and $V(t,x)$ are smooth functions that do no depend on z.

□ *Mass conservation.*
We choose a scalar test function $\varphi = \phi(t,x)$ independent of z. Then, in general for a weak solution $\underline{\vec{\boldsymbol{u}}}$ the mass conservation equation yields for all $\alpha = 1, ..., N$,

$$
\begin{aligned}
0 = & \int_{\Omega_\alpha(t)} (\nabla \cdot \underline{\vec{\boldsymbol{u}}})\, \varphi \, d\Omega \\
= & \int_{I_F(t)} \phi(t,x) \left\{ \int_{z_{\alpha-\frac{1}{2}}}^{z_{\alpha+\frac{1}{2}}} \Big(\nabla_x \cdot \underline{\vec{\boldsymbol{u}}}_H(t,x,z) + \partial_z \underline{w}(t,x,z) \Big) dz \right\} dx \\
= & \int_{I_F(t)} \phi(t,x) \left\{ \nabla_x \cdot \int_{z_{\alpha-\frac{1}{2}}}^{z_{\alpha+\frac{1}{2}}} \underline{\vec{\boldsymbol{u}}}_H(t,x,z)\, dz \ - \ \underline{\vec{\boldsymbol{u}}}^-_{H,\alpha+\frac{1}{2}} \cdot \nabla_x z_{\alpha+\frac{1}{2}} \right. \\
& \qquad \left. + \ \underline{\vec{\boldsymbol{u}}}^+_{H,\alpha-\frac{1}{2}} \cdot \nabla_x z_{\alpha-\frac{1}{2}} \ + \ \underline{w}^-_{\alpha+\frac{1}{2}} - \underline{w}^+_{\alpha-\frac{1}{2}} \right\} dx.
\end{aligned}
$$

Moreover, noticing that $\partial_t h_\alpha = \partial_t z_{\alpha+\frac{1}{2}} - \partial_t z_{\alpha-\frac{1}{2}}$, we obtain the equation

$$\begin{aligned} 0 = \int_{I_F(t)} \phi(t,x) \Big\{ & \partial_t h_\alpha \ + \ \nabla_x \cdot \big(h_\alpha \, \underline{\vec{\boldsymbol{u}}}_{H,\alpha} \big) \ - \ \partial_t z_{\alpha+\frac{1}{2}} \\ & + \partial_t z_{\alpha-\frac{1}{2}} \ - \ \underline{\vec{\boldsymbol{u}}}_{H,\alpha} \cdot \nabla_x z_{\alpha+\frac{1}{2}} \\ & + \underline{\vec{\boldsymbol{u}}}_{H,\alpha} \cdot \nabla_x z_{\alpha-\frac{1}{2}} \ + \ \underline{w}^-_{\alpha+\frac{1}{2}} - \underline{w}^+_{\alpha-\frac{1}{2}} \Big\} \, dx, \end{aligned} \tag{27}$$

for all $\phi(t,.) \in L^2(I_F(t))$.

Applying the equation (27) to $\vec{\boldsymbol{u}}$, and taking into account (8), we obtain the mass conservation laws

$$\partial_t h_\alpha + \nabla_x \cdot (h_\alpha \vec{\boldsymbol{u}}_{H,\alpha}) = G_{\alpha+\frac{1}{2}} - G_{\alpha-\frac{1}{2}}, \quad \alpha = 1, ..., N. \tag{28}$$

The quantity $G_{N+\frac{1}{2}}$ corresponds to the mass exchange at the free surface. It should be provided as data. This may corresponds, for instance, to rain effects. Otherwise it can be set to zero. Also, the quantity $G_{\frac{1}{2}}$ which represents the mass exchange at the bottom may not be null if the bottom is penetrable. It should also be provided as data.

□ *Momentum conservation.*
We consider tests functions $\vec{\boldsymbol{v}} \in H^1(\Omega_\alpha)$ verifying (26). We can develop the weak formulation (25) taking into account this structure of $\vec{\boldsymbol{v}}$ through some straightforward calculations. In these computations, we perform an integration with respect to the variable z and we identify each of the two components of the vector test functions. However, the hydrostatic pressure framework allows to drop equations that correspond to the vertical component. That is equivalent to identify the weak formulation for function tests of the form $(\vec{\boldsymbol{v}}_H, 0)'$, with $\vec{\boldsymbol{v}}_H = \vec{\boldsymbol{v}}_H(t,x)$ independent of z. Then, in general for a weak solution $\underline{\vec{\boldsymbol{u}}}$ the horizontal momentum conservation equation yields, for all $\alpha = 1, ..., N$,

$$\begin{aligned} 0 = \int_{I_F(t)} \rho \vec{\boldsymbol{v}}_H \cdot \Bigg\{ & \int_{z_{\alpha-\frac{1}{2}}}^{z_{\alpha+\frac{1}{2}}} \Big(\partial_t \underline{\vec{\boldsymbol{u}}}_{H,\alpha} + \underline{\vec{\boldsymbol{u}}}_{H,\alpha} \cdot \nabla_x \underline{\vec{\boldsymbol{u}}}_{H,\alpha} - \mu \nabla_x \cdot \big(\nabla_x \underline{\vec{\boldsymbol{u}}}_{H,\alpha} + (\nabla_x \underline{\vec{\boldsymbol{u}}}_{H,\alpha})' \big) \\ & + \nabla_x p_\alpha(t,x,z) \Big) dz \\ & + \left(\sqrt{1 + \left| \nabla_x z_{\alpha+\frac{1}{2}} \right|^2} \right) (\boldsymbol{\Sigma}^-_{T,\alpha+\frac{1}{2}} + p_{\alpha+\frac{1}{2}} \, \boldsymbol{I}) \cdot \vec{\boldsymbol{\eta}}_{\alpha+\frac{1}{2}} \\ & - \left(\sqrt{1 + \left| \nabla_x z_{\alpha-\frac{1}{2}} \right|^2} \right) (\boldsymbol{\Sigma}^+_{T,\alpha-\frac{1}{2}} + p_{\alpha-\frac{1}{2}} \, \boldsymbol{I}) \cdot \vec{\boldsymbol{\eta}}_{\alpha-\frac{1}{2}} \Bigg\} dx \end{aligned} \tag{29}$$

Applying the equation (29) to $\vec{\boldsymbol{u}}$, and taking into account (15), we obtain the

horizontal momentum conservation laws, for $\alpha = 1, ..., N$,

$$
\begin{aligned}
0 = \quad & \rho h_\alpha \partial_t \vec{\boldsymbol{u}}_{H,\alpha} \; + \; \rho h_\alpha (\vec{\boldsymbol{u}}_{H,\alpha} \cdot \nabla_x \vec{\boldsymbol{u}}_{H,\alpha}) \\
& - \nabla_x \cdot \left(\mu \, h_\alpha \big(\nabla_x \vec{\boldsymbol{u}}_{H,\alpha} + (\nabla_x \vec{\boldsymbol{u}}_{H,\alpha})' \big) \right) \; + \; \mu \left(\vec{K}_{\alpha+\frac{1}{2}} - \vec{K}_{\alpha-\frac{1}{2}} \right) \\
& + \frac{1}{2} \rho G_{\alpha+\frac{1}{2}} \left(\vec{\boldsymbol{u}}_{H,\alpha+1} - \vec{\boldsymbol{u}}_{H,\alpha} \right) \; + \; \frac{1}{2} \rho G_{\alpha-\frac{1}{2}} \left(\vec{\boldsymbol{u}}_{H,\alpha} - \vec{\boldsymbol{u}}_{H,\alpha-1} \right) \\
& + \rho g h_\alpha \nabla_x z_{\alpha-\frac{1}{2}} \; + \; \rho g \left(\sum_{\beta=\alpha+1}^{N} h_\beta \right) \nabla_x (z_{\alpha-\frac{1}{2}} - z_{\alpha+\frac{1}{2}}) \\
& + \rho g \nabla_x \left(h_\alpha \sum_{\beta=\alpha+1}^{N} h_\beta \right) \; + \; \rho g \nabla_x \left(\frac{h_\alpha^2}{2} \right) \\
& + p_S \nabla_x (z_{\alpha-\frac{1}{2}} - z_{\alpha+\frac{1}{2}}) \; + \; \nabla_x \left(h_\alpha p_S \right),
\end{aligned}
\tag{30}
$$

where the interface transference term $\vec{K}_{\alpha+\frac{1}{2}}$ comes from the decomposition of the stress tensor (15) at interface $\Gamma_{\alpha+\frac{1}{2}}$ (see Subsection 2.1.2). We have,

$$
\vec{K}_{\alpha+\frac{1}{2}} = \left(\sqrt{1 + \left| \nabla_x z_{\alpha+\frac{1}{2}} \right|^2} \right) [\widetilde{D}_{\alpha+\frac{1}{2}} \cdot \vec{\boldsymbol{\eta}}_{\alpha+\frac{1}{2}}]_H,
$$

being $[\,\cdot\,]_H$ the horizontal components of the vector. Then,

$$
\vec{K}_{\alpha+\frac{1}{2}} = \quad D_H \left(\frac{\vec{\boldsymbol{u}}^{+}_{H,\alpha+\frac{1}{2}} + \vec{\boldsymbol{u}}^{-}_{H,\alpha+\frac{1}{2}}}{2} \right) \cdot \nabla_x z_{\alpha+\frac{1}{2}} - \left(\nabla_x \left(\frac{w^{+}_{\alpha+\frac{1}{2}} + w^{-}_{\alpha+\frac{1}{2}}}{2} \right) \right)' - \vec{\mathbf{Q}}_{H,\alpha+\frac{1}{2}}.
\tag{31}
$$

Rearranging the terms in (30), using (28) to get most of them in conservative form, enables us to rewrite in each layer $\Omega_\alpha(t)$ for $\alpha = 1, ..., N$

$$
\begin{aligned}
& \rho \partial_t \left(h_\alpha \vec{\boldsymbol{u}}_{H,\alpha} \right) \; + \; \rho \nabla_x \cdot \left(h_\alpha \vec{\boldsymbol{u}}_{H,\alpha} \otimes \vec{\boldsymbol{u}}_{H,\alpha} \right) - \; \nabla_x \cdot \left(\mu \, h_\alpha \big(\nabla_x \vec{\boldsymbol{u}}_{H,\alpha} + (\nabla_x \vec{\boldsymbol{u}}_{H,\alpha})' \big) \right) \\
& = \; \frac{1}{2} \rho G_{\alpha+\frac{1}{2}} \left(\vec{\boldsymbol{u}}_{H,\alpha+1} + \vec{\boldsymbol{u}}_{H,\alpha} \right) \; - \; \frac{1}{2} \rho G_{\alpha-\frac{1}{2}} \left(\vec{\boldsymbol{u}}_{H,\alpha} + \vec{\boldsymbol{u}}_{H,\alpha-1} \right) \\
& \quad - \mu \left(\vec{K}_{\alpha+\frac{1}{2}} - \vec{K}_{\alpha-\frac{1}{2}} \right) \; - \; \rho g h_\alpha \nabla_x \left(z_B + h \right) \; - \; h_\alpha \nabla_x p_S.
\end{aligned}
\tag{32}
$$

3.1 Final system of equations and the associated energy

We introduce the kinematic viscosities $\nu = \frac{\mu}{\rho}$ and summarize here the final multilayer system, for $\alpha = 1, ..., N$,

$$
\begin{cases}
\partial_t h_\alpha + \nabla_x \cdot (h_\alpha \vec{\boldsymbol{u}}_{H,\alpha}) = G_{\alpha+\frac{1}{2}} - G_{\alpha-\frac{1}{2}}, \\
\\
\partial_t \left(h_\alpha \vec{\boldsymbol{u}}_{H,\alpha}\right) \; + \; \nabla_x \cdot (h_\alpha \vec{\boldsymbol{u}}_{H,\alpha} \otimes \vec{\boldsymbol{u}}_{H,\alpha}) \\
- \nabla_x \cdot \left(\nu \, h_\alpha \big(\nabla_x \vec{\boldsymbol{u}}_{H,\alpha} + (\nabla_x \vec{\boldsymbol{u}}_{H,\alpha})' \big) \right) \\
= \; \dfrac{1}{2} G_{\alpha+\frac{1}{2}} \left(\vec{\boldsymbol{u}}_{H,\alpha+1} + \vec{\boldsymbol{u}}_{H,\alpha} \right) \; - \; \dfrac{1}{2} G_{\alpha-\frac{1}{2}} \left(\vec{\boldsymbol{u}}_{H,\alpha} + \vec{\boldsymbol{u}}_{H,\alpha-1} \right) \\
\quad - \nu \left(\vec{K}_{\alpha+\frac{1}{2}} - \vec{K}_{\alpha-\frac{1}{2}} \right) \; - \; g h_\alpha \nabla_x \left(z_B + h \right) \; - \; \dfrac{1}{\rho} h_\alpha \nabla_x p_S.
\end{cases}
\tag{33}
$$

with $\vec{K}_{\alpha+\frac{1}{2}}$ defined by (31).

Remark 3 *Some relevant features of our model are the following:*

- *Vertical velocity: The vertical velocity plays a relevant role in our model, as it appears in the expression of the stress tensor. This is crucial to accurately model the normal momentum flux between layers.*
- *Momentum transference: We obtain that the momentum transference term can be written as*

$$
\underline{\vec{\boldsymbol{u}}}_{H,\alpha+\frac{1}{2}} G_{\alpha+1/2}, \quad \textit{with} \quad \underline{\vec{\boldsymbol{u}}}_{H,\alpha+\frac{1}{2}} = \frac{\vec{\boldsymbol{u}}_{H,\alpha+1} + \vec{\boldsymbol{u}}_{H,\alpha}}{2}.
$$

In [8] an upwind definition of $\underline{\vec{\boldsymbol{u}}}_{H,\alpha+\frac{1}{2}}$ in terms of the sign of $G_{\alpha+1/2}$ is proposed,

$$
\underline{\vec{\boldsymbol{u}}}_{H,\alpha+\frac{1}{2}} = \frac{\vec{\boldsymbol{u}}_{H,\alpha+1} + \vec{\boldsymbol{u}}_{H,\alpha}}{2} - \frac{1}{2} sign(G_{\alpha+1/2})(\vec{\boldsymbol{u}}_{H,\alpha+1} - \vec{\boldsymbol{u}}_{H,\alpha}). \tag{34}
$$

Note that if we use this definition then

$$
\begin{aligned}
\underline{\vec{\boldsymbol{u}}}_{H,\alpha+\frac{1}{2}} G_{\alpha+\frac{1}{2}} - \underline{\vec{\boldsymbol{u}}}_{H,\alpha-\frac{1}{2}} G_{\alpha-\frac{1}{2}} = \frac{\vec{\boldsymbol{u}}_{H,\alpha+1} + \vec{\boldsymbol{u}}_{H,\alpha}}{2} G_{\alpha+1/2} - \frac{\vec{\boldsymbol{u}}_{H,\alpha} + \vec{\boldsymbol{u}}_{H,\alpha-1}}{2} G_{\alpha-1/2} \\
- \left(\frac{|G_{\alpha+\frac{1}{2}}|}{2} (\vec{\boldsymbol{u}}_{H,\alpha+1} - \vec{\boldsymbol{u}}_{H,\alpha}) - \frac{|G_{\alpha-\frac{1}{2}}|}{2} (\vec{\boldsymbol{u}}_{H,\alpha} - \vec{\boldsymbol{u}}_{H,\alpha-1}) \right).
\end{aligned}
$$

Consequently, using the upwind velocity (34), yields an approximate solution of the model defined by the hydrostatic Navier-Stokes equations plus the term $\partial_z(h_\alpha \, |\mathcal{G}| \partial_z \vec{\boldsymbol{u}}_H)$, where $\mathcal{G}_{|z_{\alpha+\frac{1}{2}}} = G_{\alpha+\frac{1}{2}}$. It can be seen as a numerical viscosity term.

To end this section, let us now derive the energy equation of the model.

Proposition 1 (Energy inequality)
For the multilayer system (33)*, we denote by*

$$E_\alpha \;:=\; \frac{h_\alpha \left|\vec{\boldsymbol{u}}_{H,\alpha}\right|^2}{2} \;+\; g h_\alpha \left(z_B + \frac{h}{2}\right) \;+\; \frac{1}{\rho} h_\alpha p_S, \tag{35}$$

the energy in the layer $\Omega_\alpha(t)$, for $\alpha = 1, ..., N$. Then the model verifies the following dissipative energy inequality,

$$\begin{aligned}
&\partial_t \sum_{\alpha=1}^{N} E_\alpha \;+\; \nabla_x \cdot \left(\sum_{\alpha=1}^{N} \vec{\boldsymbol{u}}_{H,\alpha} \left(E_\alpha + g h_\alpha \frac{h}{2} \right) \right) \\
&\leq - \sum_{\alpha=1}^{N} \nu \, h_\alpha \big(|\nabla_x \vec{\boldsymbol{u}}_{H,\alpha}|^2 + |\nabla_x \cdot \vec{\boldsymbol{u}}_{H,\alpha}|^2 \big) \\
&\quad + \frac{h}{\rho} \partial_t \Big(p_S + \rho g z_B \Big) \;-\; \frac{1}{\rho} \Big(p_S + \rho g (z_B + h) + \frac{1}{2} \rho \left|\vec{\boldsymbol{u}}_{H,1}\right|^2 \Big) G_{\frac{1}{2}} \\
&\quad - \nu \, \vec{K}_{N+\frac{1}{2}} \cdot \vec{\boldsymbol{u}}_{H,N} \;+\; \nu \, \vec{K}_{\frac{1}{2}} \cdot \vec{\boldsymbol{u}}_{H,1}.
\end{aligned} \tag{36}$$

Proof: For $\alpha = 1, ..., N$, inserting the first equation of the system (33) in the second one, we obtain the equation

$$\begin{aligned}
&h_\alpha \left(\partial_t \vec{\boldsymbol{u}}_{H,\alpha} \;+\; \vec{\boldsymbol{u}}_{H,\alpha} \cdot \nabla_x \vec{\boldsymbol{u}}_{H,\alpha} \;+\; \nabla_x \left(g(z_B + h) + \frac{1}{\rho} p_S \right) \right) \\
&- \nabla_x \cdot \left(\nu_\alpha h_\alpha \big(\nabla_x \vec{\boldsymbol{u}}_{H,\alpha} + (\nabla_x \vec{\boldsymbol{u}}_{H,\alpha})' \big) \right) \\
&= \frac{1}{2} G_{\alpha+\frac{1}{2}} \left(\vec{\boldsymbol{u}}_{H,\alpha+1} - \vec{\boldsymbol{u}}_{H,\alpha} \right) \;+\; \frac{1}{2} G_{\alpha-\frac{1}{2}} \left(\vec{\boldsymbol{u}}_{H,\alpha} - \vec{\boldsymbol{u}}_{H,\alpha-1} \right) \\
&\quad - \nu \left(\vec{K}_{\alpha+\frac{1}{2}} - \vec{K}_{\alpha-\frac{1}{2}} \right).
\end{aligned} \tag{37}$$

Then we apply to the equation (37), a scalar product by $\vec{\boldsymbol{u}}_{H,\alpha}$ and we multiply the first equation of (33) by the quantity

$$\frac{\left|\vec{\boldsymbol{u}}_{H,\alpha}\right|^2}{2} \;+\; g \left(z_B + h \right) \;+\; \frac{1}{\rho} p_S,$$

and next we sum their results. That leads to the equation

$$\partial_t \left\{ h_\alpha \left(\frac{|\vec{\boldsymbol{u}}_{H,\alpha}|^2}{2} + g\left(z_B + \frac{h}{2}\right) + \frac{1}{\rho} p_S \right) \right\} \; - \; g h_\alpha \partial_t \left(z_B\right) + \tfrac{1}{2} g \left(h \partial_t h_\alpha - h_\alpha \partial_t h \right) \; - \; \frac{1}{\rho} h_\alpha \partial_t p_S$$

$$+ \nabla_x \cdot \left\{ h_\alpha \left(\frac{|\vec{\boldsymbol{u}}_{H,\alpha}|^2}{2} + g\left(z_B + h\right) + \frac{1}{\rho} p_S \right) \vec{\boldsymbol{u}}_{H,\alpha} \right\}$$

$$- \vec{\boldsymbol{u}}_{H,\alpha} \cdot \left(\nabla_x \cdot \left(\nu_\alpha h_\alpha \big(\nabla_x \vec{\boldsymbol{u}}_{H,\alpha} + (\nabla_x \vec{\boldsymbol{u}}_{H,\alpha})' \big) \right) \right)$$

$$= \left(g\left(z_B + h\right) + \frac{1}{\rho} p_S + \frac{1}{2} \vec{\boldsymbol{u}}_{H,\alpha+1} \cdot \vec{\boldsymbol{u}}_{H,\alpha} \right) G_{\alpha+\frac{1}{2}}$$

$$- \left(g\left(z_B + h\right) + \frac{1}{\rho} p_S + \frac{1}{2} \vec{\boldsymbol{u}}_{H,\alpha} \cdot \vec{\boldsymbol{u}}_{H,\alpha-1} \right) G_{\alpha-\frac{1}{2}} - \; \nu \left(\vec{K}_{\alpha+\frac{1}{2}} - \vec{K}_{\alpha-\frac{1}{2}} \right) \cdot \vec{\boldsymbol{u}}_{H,\alpha}.$$

We deduce the following energy equality per layer

$$\partial_t E_\alpha + \nabla_x \cdot \left[\vec{\boldsymbol{u}}_{H,\alpha} \left(E_\alpha + g h_\alpha \frac{h}{2} \right) \right] \; + \; \frac{1}{2} g \Big(h \partial_t h_\alpha - h_\alpha \partial_t h \Big)$$

$$- \vec{\boldsymbol{u}}_{H,\alpha} \cdot \left(\nabla_x \cdot \left(\nu \, h_\alpha \big(\nabla_x \vec{\boldsymbol{u}}_{H,\alpha} + (\nabla_x \vec{\boldsymbol{u}}_{H,\alpha})' \big) \right) \right)$$

$$= \left(g\left(z_B + h\right) + \frac{1}{\rho} p_S + \frac{1}{2} \vec{\boldsymbol{u}}_{H,\alpha+1} \cdot \vec{\boldsymbol{u}}_{H,\alpha} \right) G_{\alpha+\frac{1}{2}} \tag{38}$$

$$- \left(g\left(z_B + h\right) + \frac{1}{\rho} p_S + \frac{1}{2} \vec{\boldsymbol{u}}_{H,\alpha} \cdot \vec{\boldsymbol{u}}_{H,\alpha-1} \right) G_{\alpha-\frac{1}{2}}$$

$$- \nu \left(\vec{K}_{\alpha+\frac{1}{2}} - \vec{K}_{\alpha-\frac{1}{2}} \right) \cdot \vec{\boldsymbol{u}}_{H,\alpha} \; + \; \frac{h_\alpha}{\rho} \partial_t \Big(p_S + \rho g z_B \Big).$$

Taking into account that $\sum_{\alpha=1}^{N} h_\alpha = h$, a sum of (38) from $\alpha = 1$ to $\alpha = N$ completes the proof. □

4 Numerical approximation

The beginning of this section is devoted to the closure of the model. We restrict ourselves to a 2D flow ($d = 2$) and we re-write the model under the structure of an hyperbolic system with conservative components, nonconservative products and source terms. To that end, we set the following hypothesis on the heights of the layers for the sequel.

Assumption 1 *We consider layers having thickness proportional to the total height. That is for* $\alpha = 1, \ldots, N$, $h_\alpha = l_\alpha\, h$ *with* l_α *a positive constant. Hence we have*

$$\sum_{\alpha=1}^{N} l_\alpha = 1. \tag{39}$$

Since the horizontal domain is actually a line here, in the sequel, we shall denote the horizontal velocities $\vec{\boldsymbol{u}}_{H,\alpha}$ merely by u_α. From Assumption 1, summing the equations (28) up to $\alpha = 1, ..., N$, yields

$$G_{\alpha+\frac{1}{2}} - G_{\frac{1}{2}} = \sum_{\beta=1}^{\alpha} \left(\partial_t h_\beta + \partial_x (h_\beta u_\beta)\right)$$

and for the particular value $\alpha = N$, since $G_{N+\frac{1}{2}} = 0$, we get the global continuity equation

$$\partial_t h + \partial_x \left(h \sum_{\beta=1}^{N} l_\beta u_\beta \right) = - G_{\frac{1}{2}}. \tag{40}$$

Next, from this global continuity equation, we notice that

$$\begin{aligned} G_{\alpha+\frac{1}{2}} &= G_{\frac{1}{2}} + \sum_{\beta=1}^{\alpha} l_\beta \big(\partial_t h + \partial_x (h u_\beta)\big) \\ &= G_{\frac{1}{2}} + \sum_{\beta=1}^{\alpha} l_\beta \left(\partial_x \left(h u_\beta\right) - \sum_{\gamma=1}^{N} \partial_x \left(l_\gamma h u_\gamma\right) - \ G_{\frac{1}{2}} \right). \end{aligned}$$

Therefore we can set

$$G_{\alpha+\frac{1}{2}} = (1 - L_\alpha)\ G_{\frac{1}{2}} + \sum_{\gamma=1}^{N} \xi_{\alpha,\gamma} \partial_x (h u_\gamma), \quad \alpha = 1, \ldots, N, \tag{41}$$

where for $\alpha,\ \gamma \in \{1, \ldots, N\}$, we define $L_\alpha := l_1 + \cdots + l_\alpha$ and

$$\xi_{\alpha,\gamma} := \sum_{\beta=1}^{\alpha} (\delta_{\beta\gamma} - l_\beta) l_\gamma = \begin{cases} \big(1 - (l_1 + \cdots + l_\alpha)\big) l_\gamma & \text{if } \gamma \leq \alpha, \\ \\ -(l_1 + \cdots + l_\alpha) l_\gamma & \text{otherwise,} \end{cases}$$

where $\delta_{\beta\gamma}$ is the standard Kronecker symbol. Thus, we explicitly obtain the mass transference across interfaces in terms of the velocites in the layers.

Remark 4 *In light of* (39) *we have* $\xi_{N,\gamma} = 0$ *for all* $\gamma = 1, \ldots, N$. *In addition, setting* $\xi_{0,\gamma} = 0$ *for all* $\gamma = 1, \ldots, N$, *we notice that* $\xi_{\alpha,\gamma} = \xi_{\alpha-1,\gamma} + (\delta_{\alpha\gamma} - l_\alpha) l_\gamma$ *for all* $\alpha, \gamma = 1, \ldots, N$.

Now, using Assumption 1 and the expressions (41), the equations (32) are rewritten as

$$
\begin{aligned}
& l_\alpha \partial_t \left(h u_\alpha\right) \; + \; l_\alpha \partial_x \left(h u_\alpha^2\right) \; - \; l_\alpha \partial_x \left(2\nu \, h \partial_x u_\alpha\right) \\
& + l_\alpha \partial_x \left[h \left(\frac{1}{\rho} p_S + g \frac{h}{2} \right) \right] \; - \; l_\alpha \frac{1}{\rho} p_S \partial_x h \\
& + \sum_{\gamma=1}^{N} \frac{1}{2} \left[\left(u_\alpha + u_{\alpha-1}\right) \xi_{\alpha-1,\gamma} - \left(u_{\alpha+1} + u_\alpha\right) \xi_{\alpha,\gamma} \right] \partial_x (h u_\gamma) \\
& = - \, l_\alpha g \, h \partial_x z_B \; - \; \nu \Big(\vec{K}_{\alpha+\frac{1}{2}} - \vec{K}_{\alpha-\frac{1}{2}} \Big) \\
& \quad - \frac{1}{2} \left[\left(u_\alpha + u_{\alpha-1}\right) \left(1 - L_{\alpha-1}\right) - \left(u_{\alpha+1} + u_\alpha\right) \left(1 - L_\alpha\right) \right] G_{\frac{1}{2}},
\end{aligned}
\tag{42}
$$

for $\alpha = 1, ..., N$, where we set $L_0 = 0$ and

$$
\begin{cases}
\vec{K}_{\alpha+\frac{1}{2}} = 2 \, \partial_x u_{\alpha+\frac{1}{2}} \partial_x z_{\alpha+\frac{1}{2}} \; - \; \partial_x w_{\alpha+\frac{1}{2}} \; - \; \vec{\mathbf{Q}}_{H,\alpha+\frac{1}{2}}, \\
\\
u_{\alpha+\frac{1}{2}} := \dfrac{u^+_{\alpha+\frac{1}{2}} + u^-_{\alpha+\frac{1}{2}}}{2} \quad \text{and} \quad w_{\alpha+\frac{1}{2}} := \dfrac{w^+_{\alpha+\frac{1}{2}} + w^-_{\alpha+\frac{1}{2}}}{2}.
\end{cases}
$$

We introduce the variables $q_\alpha = h u_\alpha$ which denote the horizontal discharges in the layers $\Omega_\alpha(t)$, for $\alpha = 1, ..., N$. Therefore, from (40) and (42), we obtain the following system:

$$
\begin{cases}
\partial_t h + \partial_x \left(h \displaystyle\sum_{\beta=1}^{N} l_\beta u_\beta \right) = - \, G_{\frac{1}{2}}, \\
\\
\partial_t q_\alpha + \partial_x \left(\dfrac{q_\alpha^2}{h} + g \dfrac{h^2}{2} + \dfrac{1}{\rho} p_S h - 2\,\nu \left(\partial_x q_\alpha - \dfrac{q_\alpha}{h} \partial_x h \right) \right) \; - \; \dfrac{1}{\rho} p_S \partial_x h \\
+ \displaystyle\sum_{\gamma=1}^{N} \frac{1}{2 h l_\alpha} \Big(\left(q_\alpha + q_{\alpha-1}\right) \xi_{\alpha-1,\gamma} - \left(q_{\alpha+1} + q_\alpha\right) \xi_{\alpha,\gamma} \Big) \partial_x q_\gamma \\
= - \, g \, h \partial_x z_B \; - \; \dfrac{\nu}{l_\alpha} \Big(\vec{K}_{\alpha+\frac{1}{2}} - \vec{K}_{\alpha-\frac{1}{2}} \Big) \\
\quad - \dfrac{1}{2 h l_\alpha} \Big(\left(q_\alpha + q_{\alpha-1}\right) \left(1 - L_{\alpha-1}\right) - \left(q_{\alpha+1} + q_\alpha\right) \left(1 - L_\alpha\right) \Big) \, G_{\frac{1}{2}}.
\end{cases}
\tag{43}
$$

Remark 5 *From the definition,*

$$
\Big(\vec{K}_{\alpha+\frac{1}{2}} - \vec{K}_{\alpha-\frac{1}{2}} \Big) =
$$

$$
2 \, \partial_x u_{\alpha+\frac{1}{2}} \partial_x z_{\alpha+\frac{1}{2}} \; - \; 2 \, \partial_x u_{\alpha-\frac{1}{2}} \partial_x z_{\alpha-\frac{1}{2}} \; - \; \partial_x (w_{\alpha+\frac{1}{2}} - w_{\alpha-\frac{1}{2}}) \; - \; \Big(Q_{H,\alpha+\frac{1}{2}} - Q_{H,\alpha-\frac{1}{2}} \Big).
$$

From the computation of the vertical velocity,

$$\begin{aligned} w_{\alpha+\frac{1}{2}} - w_{\alpha-\frac{1}{2}} = & \frac{1}{2}(w^+_{\alpha+\frac{1}{2}} + w^-_{\alpha+\frac{1}{2}} - w^+_{\alpha-\frac{1}{2}} - w^-_{\alpha-\frac{1}{2}}) \\ = & \frac{1}{2}\left(2\, w^-_{\alpha+\frac{1}{2}} + (u_{\alpha+1} - u_\alpha)\partial_x z_{\alpha+\frac{1}{2}} - 2\, w^+_{\alpha-\frac{1}{2}} + (u_\alpha - u_{\alpha-1})\partial_x z_{\alpha-\frac{1}{2}}\right) \\ = & \frac{1}{2}\left((u_{\alpha+1} - u_\alpha)\partial_x z_{\alpha+\frac{1}{2}} + (u_\alpha - u_{\alpha-1})\partial_x z_{\alpha-\frac{1}{2}} - 2\, h_\alpha \partial_x u_\alpha\right). \end{aligned}$$

Noticing that $z_{\alpha+\frac{1}{2}} = z_B + L_\alpha\, h$, *we get*

$$\begin{aligned} \left(\vec{K}_{\alpha+\frac{1}{2}} - \vec{K}_{\alpha-\frac{1}{2}}\right) = & \ \partial_x(u_{\alpha+1} + u_\alpha)\,\partial_x(z_B + L_\alpha\, h) \ - \ \partial_x(u_\alpha + u_{\alpha-1})\,\partial_x(z_B + L_{\alpha-1}\, h) \ + \ \partial_x(h_\alpha \partial_x u_\alpha) \\ & - \frac{1}{2}\partial_x\Big((u_{\alpha+1} - u_\alpha)\,\partial_x(z_B + L_\alpha\, h)\Big) \ - \ \frac{1}{2}\partial_x\Big((u_\alpha - u_{\alpha-1})\,\partial_x(z_B + L_{\alpha-1}\, h)\Big) \\ & - \left(Q_{H,\alpha+\frac{1}{2}} - Q_{H,\alpha-\frac{1}{2}}\right). \end{aligned} \tag{44}$$

However, we may develop the expression (44) *to obtain*

$$\begin{aligned} \left(\vec{K}_{\alpha+\frac{1}{2}} - \vec{K}_{\alpha-\frac{1}{2}}\right) = & \ \partial_x^2(h_\alpha u_\alpha) \ - \ \frac{1}{2}(u_{\alpha+1} - u_{\alpha-1})\,\partial_x^2 z_B \ - \ \frac{1}{2}(L_\alpha u_{\alpha+1} + l_\alpha u_\alpha - L_{\alpha-1}u_{\alpha-1})\,\partial_x^2 h \\ & + \frac{1}{2}\partial_x(u_{\alpha+1} - u_{\alpha-1})\,\partial_x z_B \ + \ \frac{1}{2}\partial_x(L_\alpha u_{\alpha+1} + l_\alpha u_\alpha - L_{\alpha-1}u_{\alpha-1})\,\partial_x h \\ & - \left(Q_{H,\alpha+\frac{1}{2}} - Q_{H,\alpha-\frac{1}{2}}\right). \end{aligned} \tag{45}$$

and we can set

$$Q_{H,\alpha+\frac{1}{2}} = 2\frac{u_{\alpha+1} - u_\alpha}{h_\alpha l_\alpha + h_{\alpha+1} l_{\alpha+1}}.$$

□

The system (43) can be written in the more compact form

$$\partial_t \boldsymbol{w} + \partial_x \boldsymbol{F}(\boldsymbol{w}) + \boldsymbol{B}(\boldsymbol{w})\partial_x \boldsymbol{w} = \boldsymbol{S}(\boldsymbol{w})\partial_x H + \boldsymbol{E}(\boldsymbol{w}), \tag{46}$$

where $\boldsymbol{w} = (h, q_1, q_2, ..., q_N)^{'} \in \mathbb{R}^{N+1}$ is the unknown vector, $\boldsymbol{F} : \mathbb{R}^{N+1} \to \mathbb{R}^{N+1}$ is a regular vector function, $\boldsymbol{B} : \mathbb{R}^{N+1} \to \mathcal{M}_{N+1}(\mathbb{R})$ is a matrix function, where $\mathcal{M}_n(\mathbb{R})$ is the space of real $n \times n$ matrices ($n \in \mathbb{N}^*$), $\boldsymbol{S}, \boldsymbol{E} : \mathbb{R}^{N+1} \to \mathbb{R}^{N+1}$ are vectorial functions, and $H : \mathbb{R}^{N+1} \to \mathbb{R}$ is a real scalar function. The form (46) constitutes a classic simplified model type for multiphase or multilayer flows in the literature. Hereafter, we exhibit the algebraic expressions of the terms H, $\boldsymbol{F}(\boldsymbol{w}) = (\boldsymbol{F}_\alpha(\boldsymbol{w}))_{\alpha=0,1,...,N}$, $\boldsymbol{S}(\boldsymbol{w})$, $\boldsymbol{E}(\boldsymbol{w})$ and $\boldsymbol{B}(\boldsymbol{w}) = (\boldsymbol{B}_{\alpha,\beta}(\boldsymbol{w}))_{\alpha,\beta=0,1,...,N}$ involved in (46): $H = z_B$,

$$\boldsymbol{F}_\alpha(\boldsymbol{w}) = \begin{cases} \displaystyle\sum_{\beta=1}^{N} l_\beta q_\beta \quad \text{if } \alpha = 0 \\ \\ \dfrac{q_\alpha^2}{h} + g\dfrac{h^2}{2} - 2\,\nu\left(\partial_x q_\alpha - \dfrac{q_\alpha}{h}\partial_x h\right) + \dfrac{1}{\rho} p_S h \quad \text{if } \alpha = 1, ..., N, \end{cases}$$

$$\boldsymbol{S}_\alpha(\boldsymbol{w}) = \begin{cases} 0 \quad \text{if } \alpha = 0 \\ \\ -\,gh \quad \text{if } \alpha = 1, ..., N, \end{cases}$$

$$\boldsymbol{E}_\alpha(\boldsymbol{w}) = \begin{cases} -\,G_{\frac{1}{2}} \quad \text{if } \alpha = 0 \\ -\dfrac{1}{2hl_\alpha}\Big((q_\alpha + q_{\alpha-1})(1 - L_{\alpha-1}) - (q_{\alpha+1} + q_\alpha)(1 - L_\alpha) \Big) G_{\frac{1}{2}} \\ -\,\dfrac{\nu\left(\vec{K}_{\alpha+\frac{1}{2}} - \vec{K}_{\alpha-\frac{1}{2}}\right)}{l_\alpha} \qquad \text{if } \alpha = 1, ..., N \end{cases}$$

and

$$\boldsymbol{B}_{\alpha,\beta}(\boldsymbol{w}) = \begin{cases} 0 \quad \text{if } (\alpha,\beta) \in \{0\} \times \{0, 1, ..., N\} \\ \\ -\,\dfrac{1}{\rho} p_S \quad \text{if } (\alpha,\beta) \in \{1, ..., N\} \times \{0\} \\ \\ \dfrac{1}{2hl_\alpha}\Big((q_\alpha + q_{\alpha-1})\,\xi_{\alpha-1,\beta} - (q_{\alpha+1} + q_\alpha)\,\xi_{\alpha,\beta} \Big) \quad \text{if } \alpha, \beta = 1, ..., N \end{cases}$$

The equation (46) can be reformulated as

$$\partial_t \boldsymbol{w} \;+\; \boldsymbol{A}(\boldsymbol{w})\partial_x \boldsymbol{w} \;=\; \boldsymbol{S}(\boldsymbol{w})\partial_x H + \boldsymbol{E}(\boldsymbol{w}),$$

where $\boldsymbol{A}(\boldsymbol{w}) = \boldsymbol{B}(\boldsymbol{w}) + \boldsymbol{J}(\boldsymbol{w})$ with $\boldsymbol{J}(\boldsymbol{w}) = \dfrac{\partial \boldsymbol{F}(\boldsymbol{w})}{\partial \boldsymbol{w}}$ the Jacobian matrix of $\boldsymbol{F}$. The matrix $\boldsymbol{J}(\boldsymbol{w}) = (\boldsymbol{J}_{\alpha,\beta}(\boldsymbol{w}))_{\alpha,\beta=0,1,...,N} \in \mathcal{M}_{(N+1)}(\mathbb{R})$ is given by

$$\boldsymbol{J}_{\alpha,\beta}(\boldsymbol{w}) = \begin{cases} 0 \quad \text{if } (\alpha,\beta) = (0,0) \\ \\ l_\beta \quad \text{if } (\alpha,\beta) \in \{0\} \times \{1, ..., N\} \\ \\ -\dfrac{q_\alpha^2}{h^2} - 2\,\nu\dfrac{q_\alpha}{h^2}\partial_x h + gh + \dfrac{1}{\rho} p_S \quad \text{if } (\alpha,\beta) \in \{1, ..., N\} \times \{0\} \\ \\ \dfrac{2}{h}\Big(q_\alpha + \nu\,\partial_x h\Big)\delta_{\alpha\beta} \quad \text{if } \alpha, \beta = 1, ..., N. \end{cases}$$

The numerical approximation of this model is based on a standard finite volume method combined with a two-step splitting procedure. The splitting consists in ruling out, from the first step, the contribution of the source term $\boldsymbol{E}(\boldsymbol{w})$ in (46). The procedure is detailed hereafter. In the first step, we subdivide the horizontal spatial domain into standard computational cells $I_i = [x_{i-1/2}, x_{i+1/2}]$, and then apply a finite volume scheme for (46), where we exclude the contributions of the source term in $\boldsymbol{E}(\boldsymbol{w})$ by subtracting it from the right-hand side. The resulting system has the form

$$\boldsymbol{W}_t + \mathcal{A}\big(\boldsymbol{W}\big) \cdot \boldsymbol{W}_x = 0, \tag{47}$$

where $\boldsymbol{W}$ is the concatenated vector $\boldsymbol{W} := (\boldsymbol{w}, H)^{\mathrm{t}} \in \Omega \subset \mathbb{R}^{N+1}$. Solutions of (47) may develop discontinuities and, due to the non-divergence form of the equations, the notion of weak solution in the sense of distributions cannot be used. The theory introduced by Dal Maso, LeFloch, and Murat [11] is followed here to define weak solutions. This theory allows one to define the nonconservative product $\mathcal{A}(\boldsymbol{W}) \cdot \boldsymbol{W}_x$ as a bounded measure provided a family of Lipschitz continuous paths $\Psi : [0,1] \times \Omega \times \Omega \to \Omega$ is prescribed, which must satisfy certain natural regularity conditions, in particular

$$\Psi\big(0; \boldsymbol{W}_{\mathrm{L}}, \boldsymbol{W}_{\mathrm{R}}\big) = \boldsymbol{W}_{\mathrm{L}}, \qquad \Psi\big(1; \boldsymbol{W}_{\mathrm{L}}, \boldsymbol{W}_{\mathrm{R}}\big) = \boldsymbol{W}_{\mathrm{R}},$$

and

$$\Psi\big(s; \boldsymbol{W}, \boldsymbol{W}\big) = \boldsymbol{W} \quad \text{for all } s \in [0,1].$$

For example, a family of straight segments can be considered:

$$\Psi\big(s; \boldsymbol{W}_{\mathrm{L}}, \boldsymbol{W}_{\mathrm{R}}\big) = \boldsymbol{W}_{\mathrm{L}} + s\big(\boldsymbol{W}_{\mathrm{R}} - \boldsymbol{W}_{\mathrm{L}}\big), \quad s \in [0,1].$$

We consider here path-conservative numerical schemes in the sense defined by Parés in [15]. Applied to the system (46), the scheme is of the form

$$\boldsymbol{w}_i^{n+1/2} = \boldsymbol{w}_i^n - \frac{\Delta t}{\Delta x}\left(\mathcal{F}_{i+1/2}^n - \mathcal{F}_{i-1/2}^n + \frac{1}{2}\big(\mathcal{B}_{i+1/2}^n + \mathcal{B}_{i-1/2}^n\big)\right), \tag{48}$$

where the expressions $\mathcal{F}_{i+1/2}^n$ and $\mathcal{B}_{i+1/2}^n$ are defined as follows:

$$\begin{aligned} \mathcal{F}_{i+1/2}^n := \;& \tfrac{1}{2}\big(\boldsymbol{F}(\boldsymbol{w}_i^n) + \boldsymbol{F}(\boldsymbol{w}_{i+1}^n)\big) \\ & - \tfrac{1}{2}\boldsymbol{Q}_{i+1/2}^n \left(\boldsymbol{w}_{i+1}^n - \boldsymbol{w}_i^n - \boldsymbol{\Lambda}_{i+1/2}^n \boldsymbol{S}_{i+1/2}^n \big(H_{i+1}^n - H_i^n\big)\right), \end{aligned}$$

$$\mathcal{B}_{i+1/2}^n = \boldsymbol{B}_{i+1/2}^n\big(\boldsymbol{w}_{i+1}^n - \boldsymbol{w}_i^n\big) - \boldsymbol{S}_{i+1/2}^n\big(H_{i+1}^n - H_i^n\big). \tag{49}$$

We recall that (cf. [16, 18]) if Ψ denotes a family of Lipschitz continuous paths used to design the path-conservative scheme (48), for a given matrix $\boldsymbol{C}$, we denote by $\boldsymbol{C}_\Psi$ its Roe linearization and set

$$\boldsymbol{C}_{i+1/2}^n = \boldsymbol{C}_\Psi\big(\boldsymbol{W}_{i+1}^n, \boldsymbol{W}_i^n\big).$$

The matrix $\boldsymbol{\Lambda}(\boldsymbol{w})$ represents an approximation of the inverse of $\boldsymbol{A}(\boldsymbol{w}) = \boldsymbol{J}(\boldsymbol{w}) + \boldsymbol{B}(\boldsymbol{w})$, where $\boldsymbol{J}(\boldsymbol{w})$ is the Jacobian matrix of the flux vector $\boldsymbol{F}(\boldsymbol{w})$ (see above). In addition, $\boldsymbol{Q}_{i+1/2}^n$ is the numerical viscosity matrix whose definition identifies the particular finite volume method used. For example, the Roe method is

defined by $\boldsymbol{Q}_{i+1/2} = |\boldsymbol{A}_{i+1/2}|$, where $\boldsymbol{A}_{i+1/2}$ is the Roe matrix defined in the sense of Toumi (see [16, 18]). An interesting alternative to Roe method for system with a great number of unknowns are PVM ("polynomial viscosity matrix") methods (see [9]). At this step, we obtain from (48) the intermediate solution

$$\boldsymbol{w}_i^{n+1/2} = \big(h_i^{n+1/2},\ \boldsymbol{q}_i^{n+1/2}\big)^{\mathrm{t}},$$

where

$$\boldsymbol{q}_i^{n+1/2} = \big((q_1)_i^{n+1/2}, \ldots, (q_N)_i^{n+1/2}\big)^{\mathrm{t}}.$$

Next, in the second step, we complete the numerical procedure by including the contribution of the source term expressed by the matrix $\boldsymbol{E}(\boldsymbol{w})$ in the right-hand side of (46). More precisely, we merely resolve the following implicit update:

$$\boldsymbol{w}_i^{n+1} = \boldsymbol{w}_i^{n+1/2} + \Delta t\, \boldsymbol{E}\big(\boldsymbol{w}_i^{n+1}\big). \tag{50}$$

Remark 6 *We recall that the source terms matrix $\boldsymbol{E}(\boldsymbol{w})$ represents the contributions of the frictions at the interfaces together with the mass flux exchange at the bottom interface. Hence if we assume a non penetrable bottom layer and neglect those frictions, the source terms matrix $\boldsymbol{E}(\boldsymbol{w})$ vanishes and then the splitting process is no more necessary. Therefore we actually meet, in this case,*

$$\boldsymbol{w}_i^{n+1} = \boldsymbol{w}_i^{n+1/2}.$$

5 Numerical tests

We present in this section some simulations with the model designed in the previous section. We start by a variation of a standard test simulating different stationary flow regimes and next, we compare the model with a finite element Navier-Stokes model, computed with the FreeFem++ library [14]. In both tests the objective is to analyze the accuracy of the computation of the vertical velocity. We also test the ability of our model to reproduce re-circulations of the flow past an obstacle.

5.1 Test 1: A variant of a classic test

In this test we set as initial condition water solution at rest over a bump. Then, we impose a boundary condition until it reaches a stationary solution. For the shallow water equations it is a classic test, by imposing a constant inflow (see [4, 8, 10, 13]). The multilayer approach allows us to introduce a variation of this test, by considering a constant in time inflow with a linear vertical profile. Moreover, this approach allows us to observe the influence of the vertical viscosity effects in the solution. With this aim first we neglect the viscosity effects, i.e. $\nu = 0$, and secondly we set $\nu = 10^{-3}$.

Actually we consider a channel of horizontal length $L = 20\,\mathrm{m}$, which we discretize with $n = 400$ cells in the horizontal direction. The vertical direction is discretized using

$N = 10$ horizontal layers with a CFL number equal to 0.8 and we neglect frictions at the free surface and the bottom. The bottom elevation is given by

$$z_{\mathrm{B}}(x) = \max\left(0,\ 0.2\ - 0.05(x-10)^2\right).$$

The initial conditions are given by

$$h(t=0) = 0.33 - z_{\mathrm{B}} \quad \text{and} \quad q(t=0) = 0,$$

The boundary conditions are

$$\partial_x h = 0; \quad q_\alpha = \tfrac{0.36}{m}(\alpha - 1); \quad \text{inflow } (x=0)$$

$$h = 0.33; \quad \partial_x q_\alpha = 0; \quad \text{outflow } (x=L)$$

In Figure 2 we present the solution at $t = 15$, 20 and 150 s, for the free surface and the velocity vectors when $\nu = 0$. Moreover, we compare the maximum of the absolute value of the vertical component of the velocity when it is computed via the algorithm proposed in this paper and via a simple post-processing of the incompressibility condition (i.e. to consider (21) with $w^-_{\alpha+\frac{1}{2}} = w^+_{\alpha-\frac{1}{2}}$). We observe that some small differences appear between both approximations near the bump for $t = 150$ s. In the pictures the head of the vectors are proportional to its norm.

In Figure 4 we compare the evolution of the free surface and the velocity vectors at $t = 15$, 20 and 150 s when $\nu = 10^{-3}$. First we observe a large influence on the discontinuity that appears in the free surface for $\nu = 0$. Second, we observe that for $\nu = 10^{-3}$ the multilayer approach allows to recover a small recirculation of the fluid at the right of the bump (see Figure 3).

Figures 4(a), 4(c) and 4(e) correspond to the velocity vectors obtained with the algorithm proposed in this paper. Figures 4(b), 4(d) and 4(f) correspond to the velocity vectors whose vertical component is obtained by a simple post-processing of the incompressibility condition. We observe that the direction and length of the velocity vectors near the bump depend on the algorithm to compute the vertical velocity. Let us remark that the horizontal component of the velocity vectors in both cases are the same, so the differences appear in their vertical component. It can be observed for example when we compare the zoom corresponding to figures 4(e) and 4(f).

In Figure 5 we compare the maximum absolute value of the vertical component of the velocity computed with both algorithms. In Figure 5(d) we present the maximum absolute value of the difference between these two approximations of the vertical velocity component. We observe that for this test near the bump there exist significant differences between them.

5.2 Test 2: Comparison with Navier-Stokes

The main objective of this test is to compare the vertical velocity computed by a post-processing of the incompressibility condition with the one obtained using the algorithm we propose. We consider a simple test to compare both type of approximations of the vertical velocity with the one obtained by a standard finite element solution of the Navier-Stokes equations. First, we consider the evolution of the multilayer model until a stationary solution. Then, we set the stationary domain to compute the corresponding stationary solution as an approximation of the full N-S equation. We compute this stationary solution with a Taylor-Hood $P2-P1$ finite element formulation implemented in the FreeFem++ library [14].

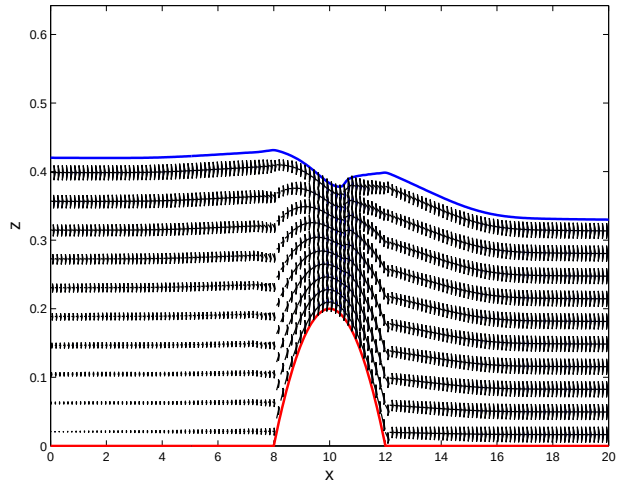

(a) Model. $t = 15$ s.

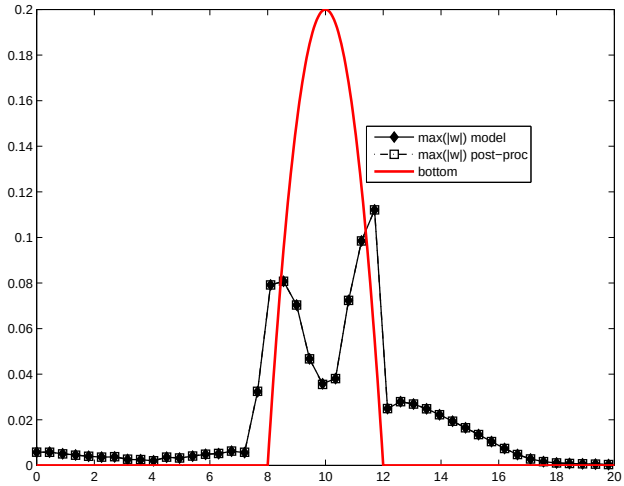

(b) Comp. $max(|w|)$ $t = 15$ s.

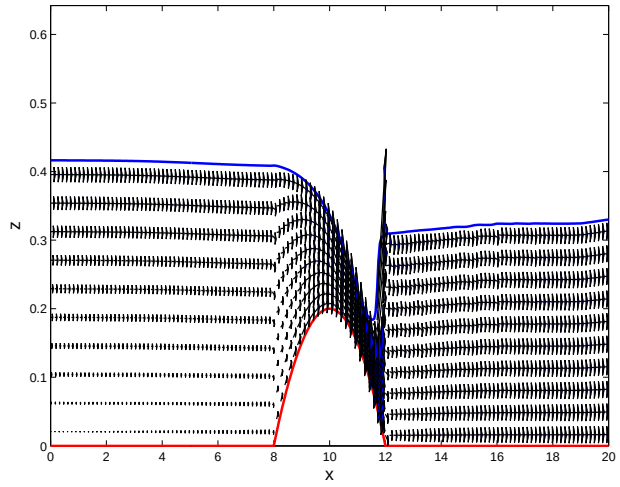

(c) Model. $t = 20$ s.

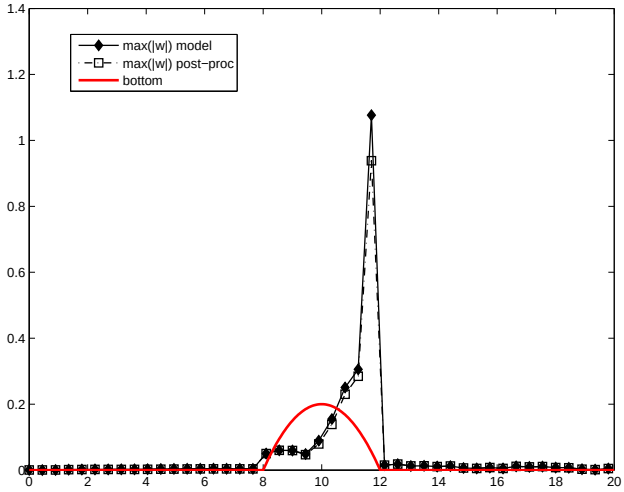

(d) Comp. $max(|w|)$ $t = 20$ s.

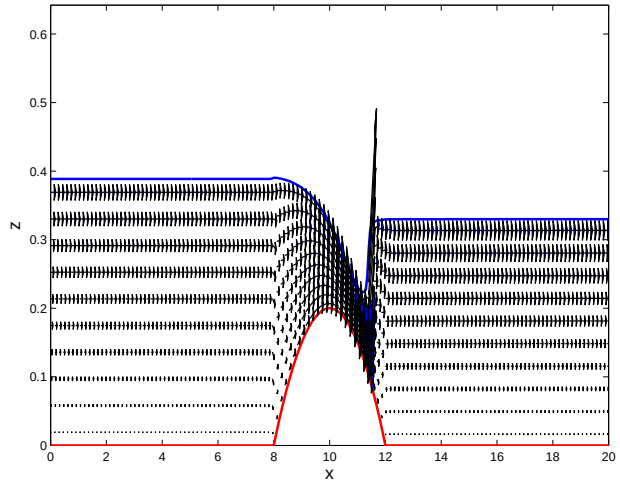

(e) Model. $t = 150$ s.

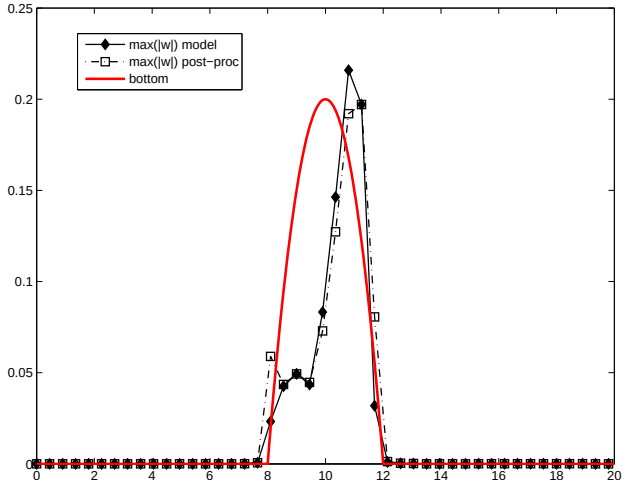

(f) Comp. $max(|w|)$ $t = 150$ s.

Figure 2: Test 1. Left: Free surface evolution and velocity vectors for $\nu = 0$. Right: Comparison of max($|w|$), when computed with the model and by a post-processing of the incompressibility condition.

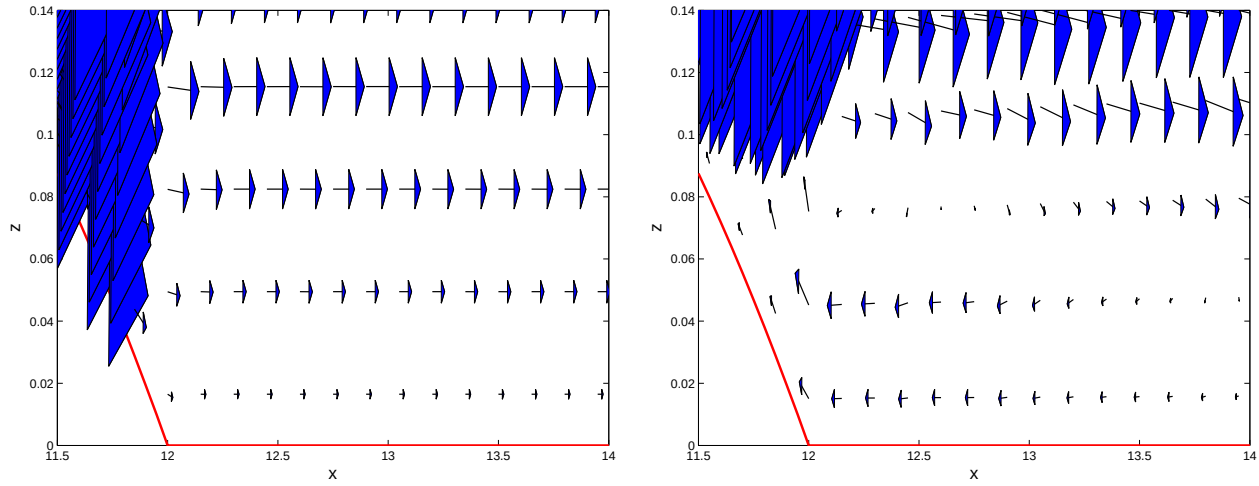

(a) $\nu = 0$, $t = 150$ s. (b) $\nu = 10^{-3}$, $t = 150$ s.

Figure 3: Test 1. Zoom at the right of the bump, $t = 150$ s. Left: Velocity vectors for $\nu = 0$. Right: Velocity vectors for $\nu = 10^{-3}$

We consider a channel of horizontal length $L = 3$ m, which we discretize with $n = 200$ cells in the horizontal direction in the multilayer model. The vertical direction is discretized using $N = 10$, $N = 20$ and $N = 30$ layers with a CFL number equal to 0.8. We test various kinematic viscosity coefficients and we present here results for $\nu = 5.10^{-4}$, $10^{-3}\,\mathrm{m}^2 \cdot \mathrm{s}^{-1}$. In the multilayer model, as the Navier-Stokes equations, frictions are only induced by the viscous term as depicted in Section 2. Actually, the viscous term of the model involves a vertical variation of the velocity at the interfaces. Here, we neglect frictions at the free surface and at the bottom.

The bottom elevation is defined by

$$z_{\mathrm{B}}(x) = \begin{cases} 0 & \text{if} \quad x \leq 1, \\ 0.5\,(x-1) & \text{if} \quad 1 \leq x \leq 2, \\ 0.5 & \text{if} \quad x \geq 2. \end{cases}$$

As boundary conditions, we consider open vertical boundaries and we impose, at the left, a fixed horizontal velocity which is linear in the z direction.

$$q(0,t) = \bar{q}\,\frac{2\,z}{h(0,t)}.$$

We have simulated several values of the mean inflow $\bar{q}$ with initial conditions given by

$$h(t=0) = 1\,\mathrm{m} - z_{\mathrm{B}} \quad \text{and} \quad q(t=0) = 0\,\mathrm{m}^2 \cdot \mathrm{s}^{-1}.$$

The fluid domain (in figure 6(a)) resulting at the stationary state of the multilayer system stands for the domain data of the FreeFem++ Navier-Stokes (NS-ff++) simulation. Since the horizontal velocity of the model is constant per layer, we compare the values with the FreeFem++ horizontal velocity first, evaluated at the middle point of

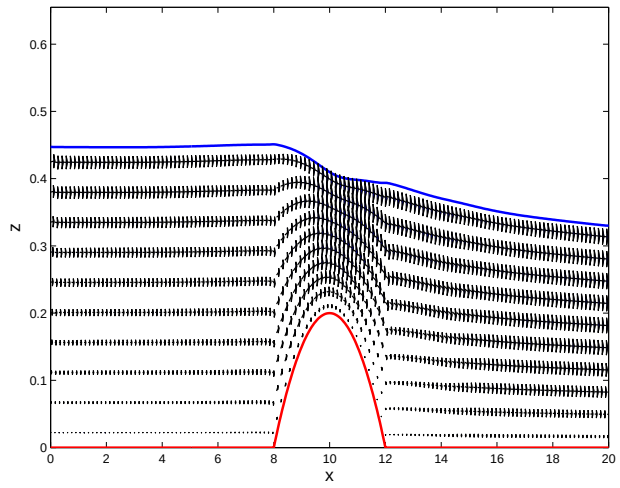

(a) Model. $t = 15$ s.

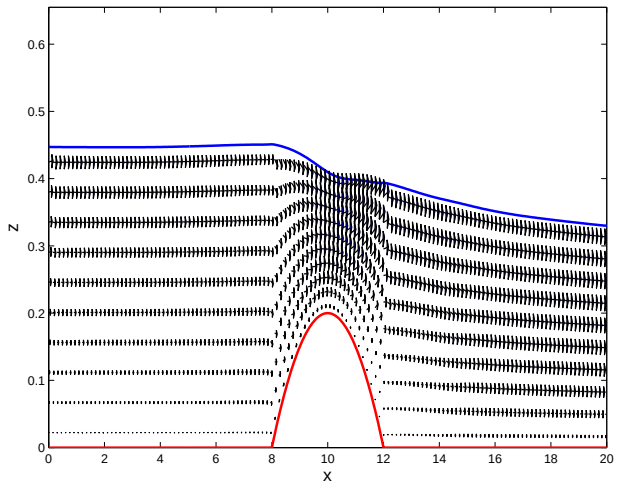

(b) Post-proc. $t = 15$ s.

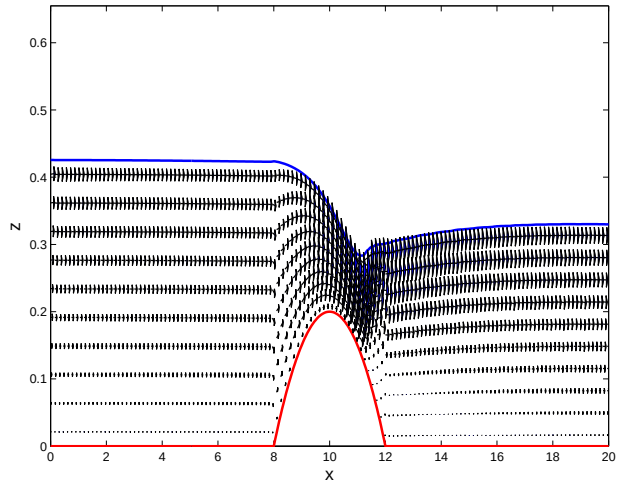

(c) Model. $t = 150$ s.

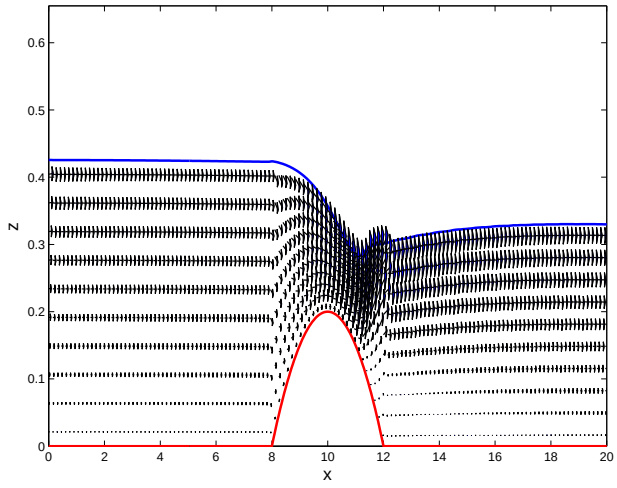

(d) Post-proc. $t = 150$ s.

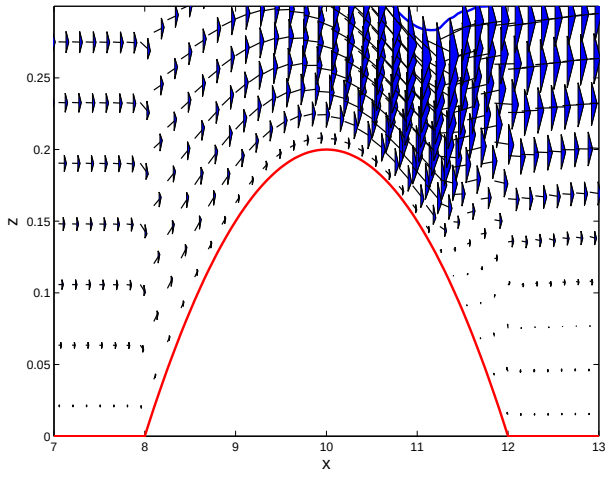

(e) Model. $t = 150$ s. Zoom

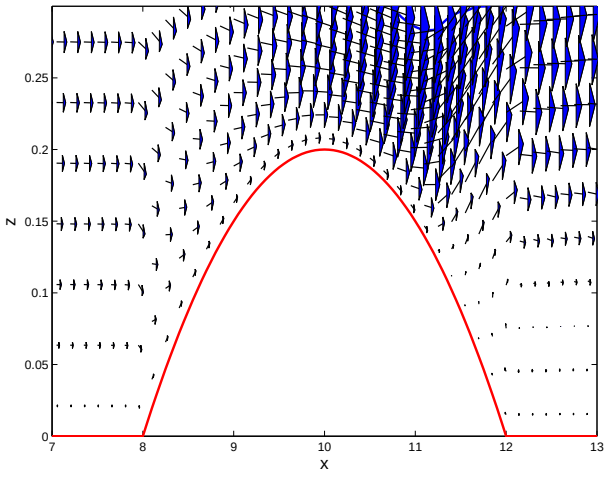

(f) Post-proc. $t = 150$ s. Zoom

Figure 4: Test 1. Free surface evolution and velocity vectors for $\nu = 10^{-3}$. Left: Model, Right: velocity vectors corresponding to a vertical velocity computed via a simple post-processing of the incompressibility condition.

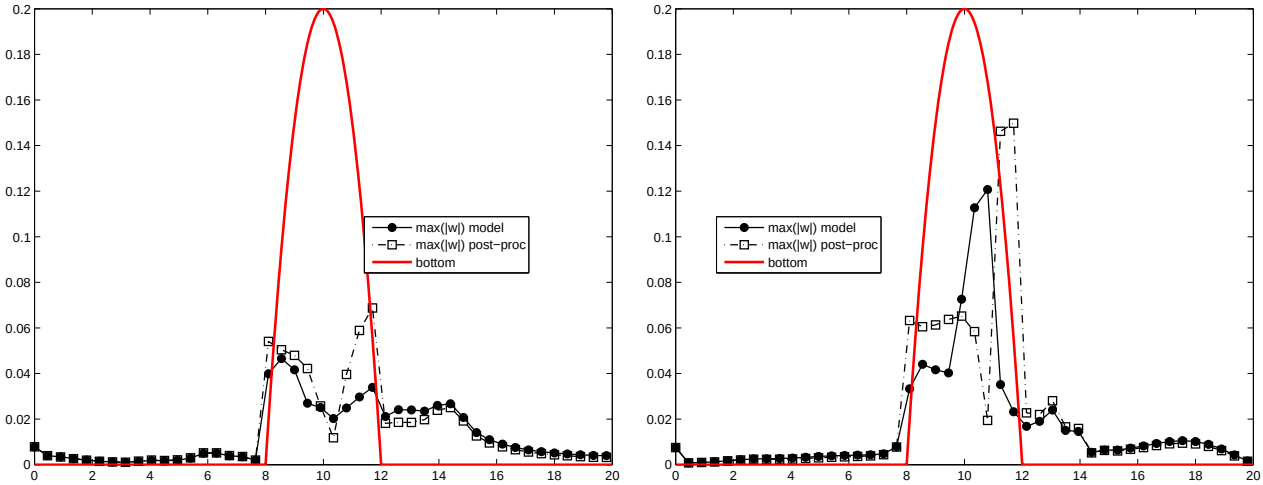

(a) Comp. $max(|w|)$ $t = 15$ s.

(b) Comp. $max(|w|)$ $t = 20$ s.

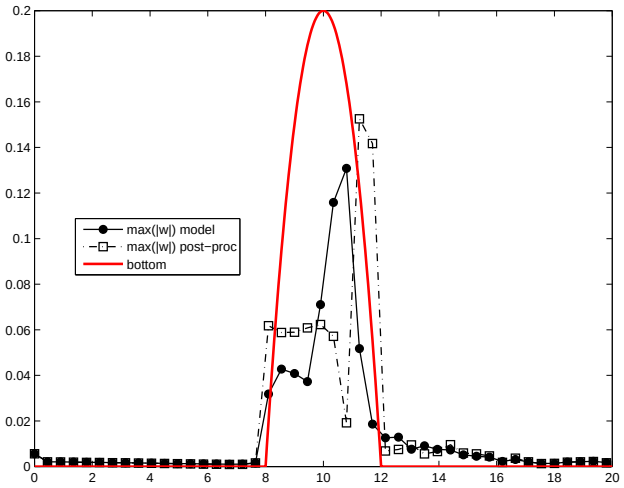

(c) Comp. $max(|w|)$ $t = 150$ s.

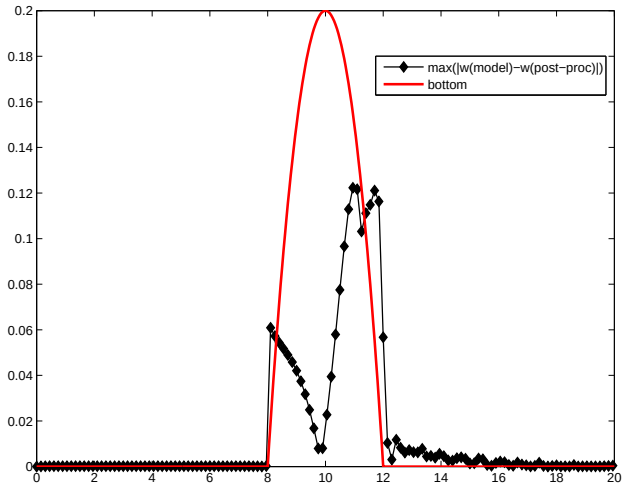

(d) $max(|w_{model} - w_{post-proc}|)$ $t = 150$ s.

Figure 5: Test 1: Maximum and minimum values of w. Comparison between the values obtained with the proposed model and a simple post-processing of the incompressibility equation.

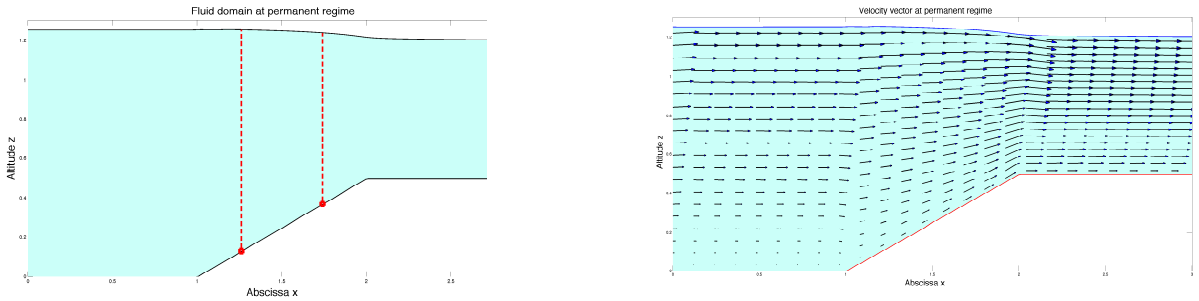

(a) Fluid domain (b) Velocity vector

Figure 6: Fluid domain and velocity vector at the stationary regime for a viscosity $\nu = 5.10^{-4}\,\mathrm{m}^2 \cdot \mathrm{s}^{-1}$ and a mean inflow $\bar{q} = 1\,\mathrm{m}^2 \cdot \mathrm{s}^{-1}$. The viscous term is considered at the bottom.

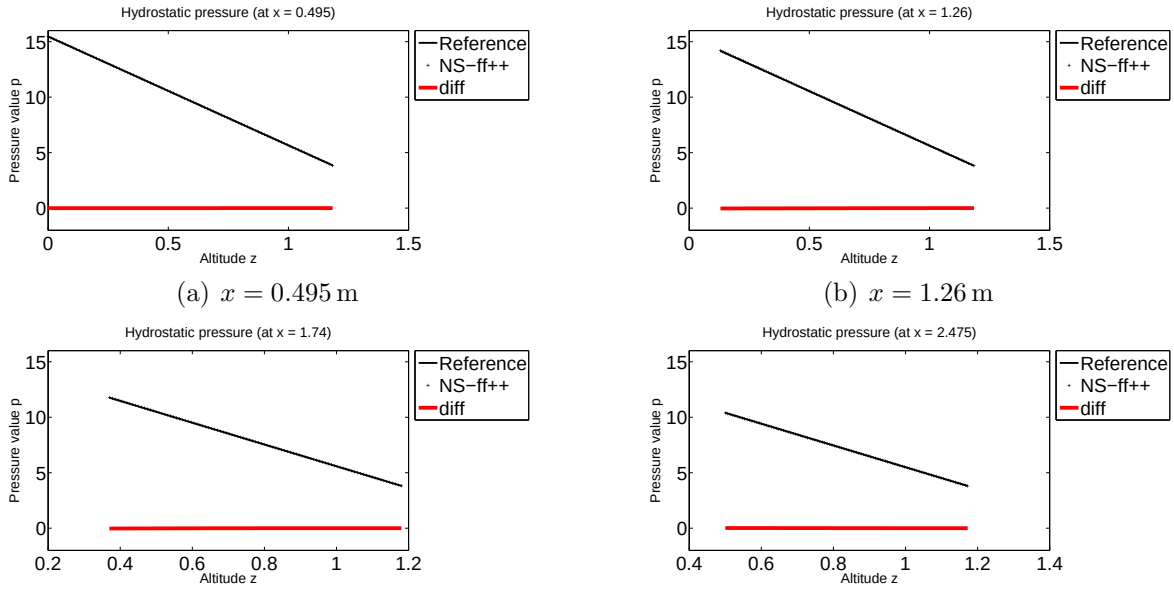

(a) $x = 0.495\,\mathrm{m}$ (b) $x = 1.26\,\mathrm{m}$

(c) $x = 1.74\,\mathrm{m}$ (d) $x = 2.475\,\mathrm{m}$

Figure 7: Comparing NS-ff++ simulation pressure with theoretical hydrostatic pressure for viscosity $\nu = 10^{-3}\,\mathrm{m}^2 \cdot \mathrm{s}^{-1}$ and mean inflow $\bar{q} = 0.5\,\mathrm{m}^2 \cdot \mathrm{s}^{-1}$.

the layer and next, averaged in the layer. The vertical velocity of the model is compared with the vertical velocity of the FreeFem++ Navier-Stokes and the standard vertical velocity computed with a postprocessing technique using the divergence-free condition and the kinematic condition at the bottom (see [8]). We make these comparisons at some selected positions x along the channel. We pick out positions along the slope and we present here the results for two $x = 1.26$ and $x = 1.74\,\mathrm{m}$ (See Figure 6(a)). First we have checked and established that FreeFem++ simulations are in a hydrostatic framework by comparing the pressure value with the theoretical expression $p(x, z) = p(x, z_B + h) + \rho g(z_B + h - z)$. In Figure 7, we show an example of results for the pressure at four positions $x = 0.495$, 1.26, 1.74, $2.475\,\mathrm{m}$. Actually we plot the pressure curves together with their pointwise difference. We can conclude that for this test we have a hydrostatic pressure, that allow us to compare the numerical results corresponding to the approximation of the full N-S equations by finite element methods and the multilayer aproaches.

We may observe (figures 8 - 12) a quite satisfactory approximation of the full Navier-Stokes solution by the model proposed in this work. For small values of z the differences can correspond to the form in which boundary conditions are imposed in the Freefem++ finite element code for Navier-Stokes and the Finite Volume one for the multilayer model. Especially, we notice that the vertical velocity drawn from the model is more accurate than the one obtained by the usual post-processing technique. Let us recall that the vertical velocity from the model is piecewise linear in z per layer. That explains the features we see on the pictures where we notice decreasing jumps at the interfaces as the number of layers increases. Actually, in the pictures of the vertical velocities, we plot the values of the post-processing at the middle altitude of each layer while for the model, we plot the full range of values together with an emphasizing of the values at the layer's middle altitude.

Let us comment the numerical results obtained with viscosity $\nu = 5.10^{-4}\ \mathrm{m}^2 \cdot \mathrm{s}^{-1}$ and mean inflow $\bar{q} = 0.5\,\mathrm{m}^2 \cdot \mathrm{s}^{-1}$. In Figure 8 we compare the numerical results obtained for the horizontal velocities at $x = 1.26$ and $x = 1.74$ m. In Figure 9 the numerical results for the vertical velocity are presented.

If we compare the multilayer models for $N = 10$, $N = 20$ and $N = 30$ (Figure 8 for the horizontal velocities and Figure 9 for the vertical velocity) we can observe some differences between the numerical results corresponding to $N = 10$ and $N = 20$. There is a smaller difference when we compare the numerical results corresponding to $N = 20$ and $N = 30$. Let us remark that to increase the number of layer is equivalent to do a mesh refinement in vertical. Then, is satisfactory to obtain a number of layers N from which the solution is nearly refinement-independent. So, with the purpose of brevity in the exposition we will only comment the numerical results corresponding to $N = 20$ in the forthcoming cases.

The first conclusion is that the horizontal velocities are rather accurate (see Figure 8). For the vertical velocity (Figure 9) we observe that the numerical results obtained with the algorithm that we propose in this work have also a good agreement with the ones obtained using the finite element solution of the full model. However, the vertical velocity obtained by a simple post-processing of the incompressibility condition is far from the finite element one.

In figures 9(a) and 9(b) we point out the position of the jumps in the vertical profile of our multilayer model. Note that if we neglect the discontinuity in these interfaces then we obtain the same vertical profile as with the post-processing approach. So we remark the necessity to compute this jump in the profile of the vertical profile by the normal flux jump condition.

We obtain a similar conclusion when we consider some other values of ν and $\bar{q}$. In

Figure 10 we show the horizontal and vertical velocity profiles at $x = 1.26$ and $x = 1.74$ for $\nu = 5.10^{-4}\,\mathrm{m}^2 \cdot \mathrm{s}^{-1}$ and $\bar{q} = 1\,\mathrm{m}^2 \cdot \mathrm{s}^{-1}$. Figure 11 corresponds to $\nu = 10^{-3}\,\mathrm{m}^2 \cdot \mathrm{s}^{-1}$, $\bar{q} = 0.5\,\mathrm{m}^2 \cdot \mathrm{s}^{-1}$. Figure 12 corresponds to $\nu = 10^{-3}\,\mathrm{m}^2 \cdot \mathrm{s}^{-1}$, $\bar{q} = 1\,\mathrm{m}^2 \cdot \mathrm{s}^{-1}$.

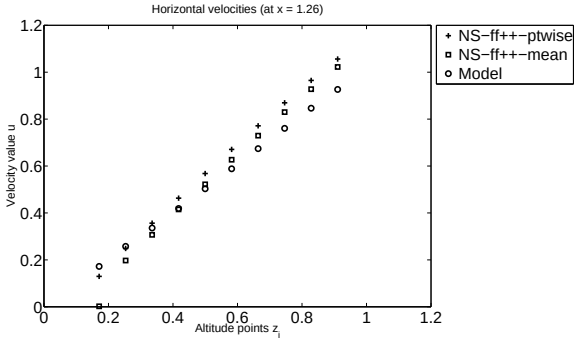

(a) $N = 10$, $x = 1.26$

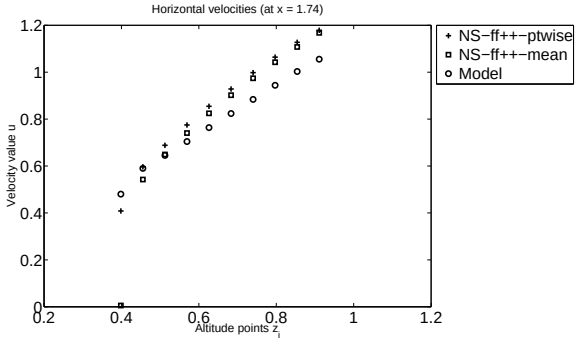

(b) $N = 10$, $x = 1.74$

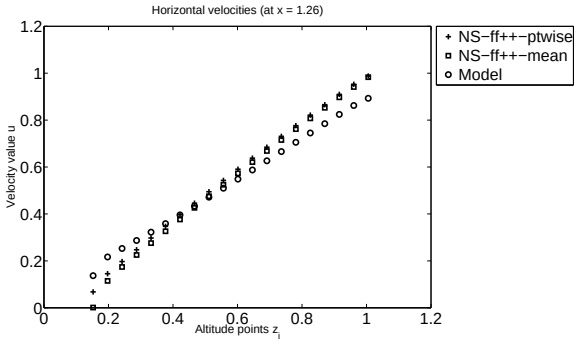

(c) $N = 20$, $x = 1.26$

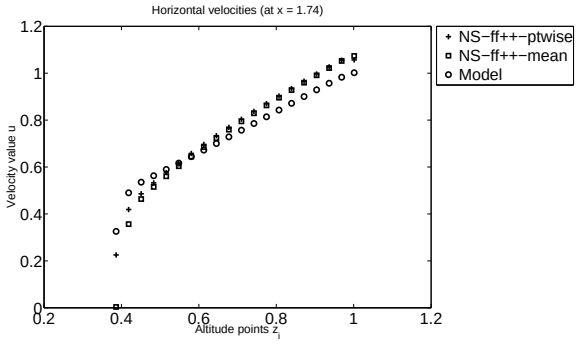

(d) $N = 20$, $x = 1.74$

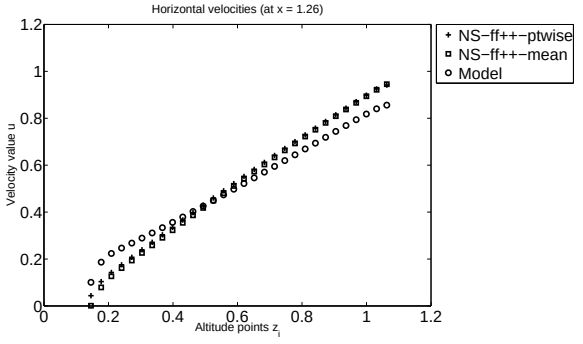

(e) $N = 30$, $x = 1.26$

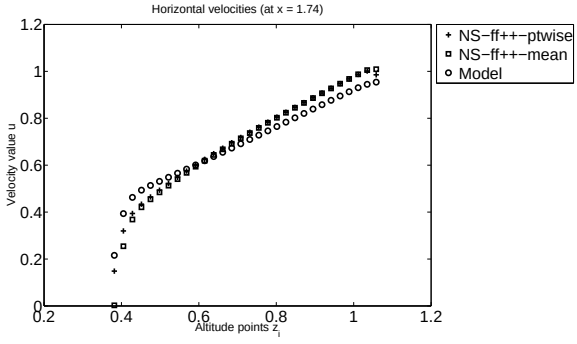

(f) $N = 30$, $x = 1.74$

Figure 8: Horizontal velocities at the positions $x = 1.26\,\mathrm{m}$ and $x = 1.74\,\mathrm{m}$ with viscosity $\nu = 5.10^{-4}\,\mathrm{m}^2 \cdot \mathrm{s}^{-1}$ and mean inflow $\bar{q} = 0.5\,\mathrm{m}^2 \cdot \mathrm{s}^{-1}$.

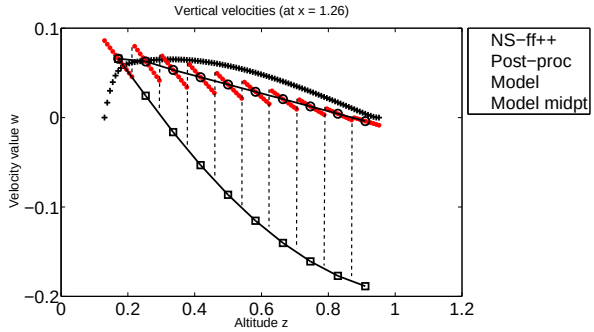

(a) $N = 10$, $x = 1.26$

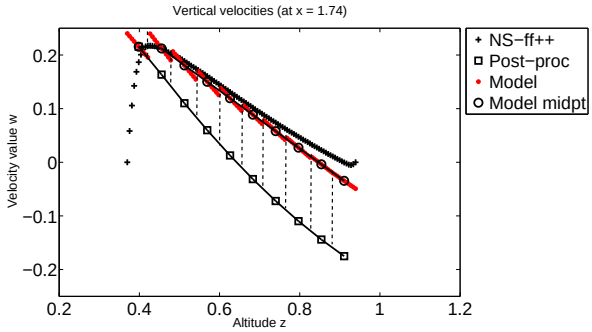

(b) $N = 10$, $x = 1.74$

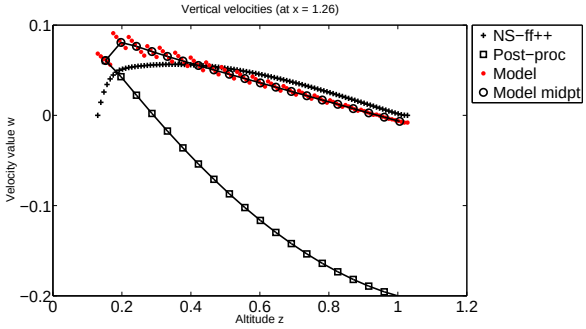

(c) $N = 20$, $x = 1.26$

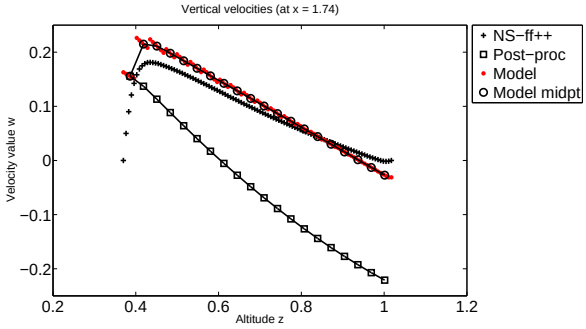

(d) $N = 20$, $x = 1.74$

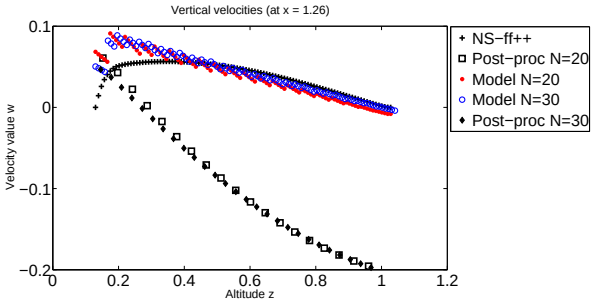

(e) Comp. $N = 20$ and $N = 30$, $x = 1.26$

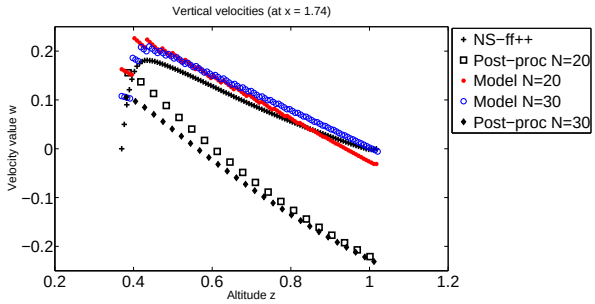

(f) Comp. $N = 20$ and $N = 30$, $x = 1.74$

Figure 9: Vertical velocities at the positions $x = 1.26\,\mathrm{m}$ and $x = 1.74\,\mathrm{m}$ with viscosity $\nu = 5.10^{-4}\,\mathrm{m}^2 \cdot \mathrm{s}^{-1}$ and mean inflow $\bar{q} = 0.5\,\mathrm{m}^2 \cdot \mathrm{s}^{-1}$.

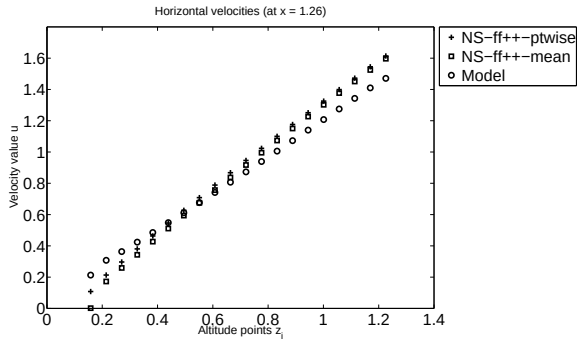

(a) Horizontal Vel. $x = 1.26$

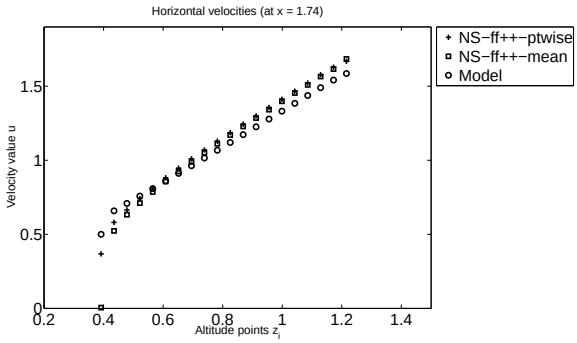

(b) Horizontal Vel. $x = 1.74$

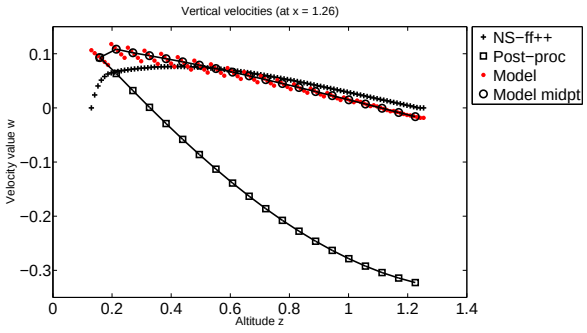

(c) Vertical Vel. $x = 1.26$

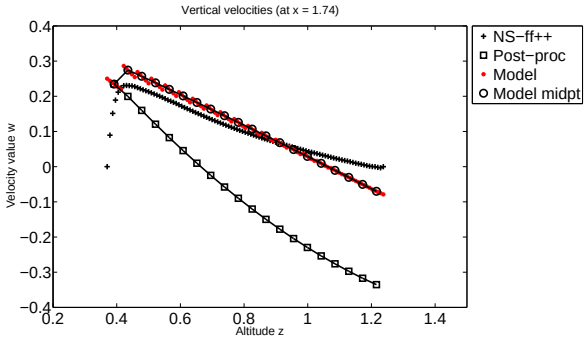

(d) Vertical Vel. $x = 1.74$

Figure 10: Horizontal and Vertical velocities at the positions $x = 1.26$ and $x = 1.74$ with viscosity $\nu = 5.10^{-4}\,\mathrm{m}^2 \cdot \mathrm{s}^{-1}$ and mean inflow $\bar{q} = 1\,\mathrm{m}^2 \cdot \mathrm{s}^{-1}$. ($N = 20$).

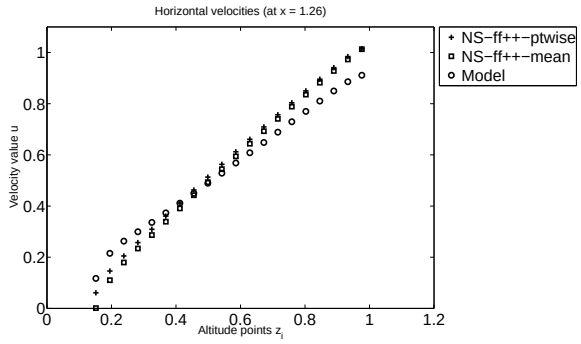

(a) Horizontal Vel. $x = 1.26$

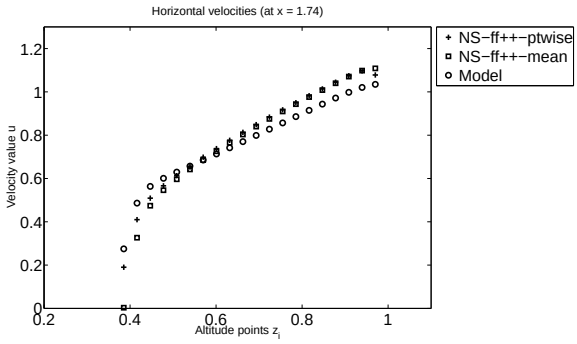

(b) Horizontal Vel. $x = 1.74$

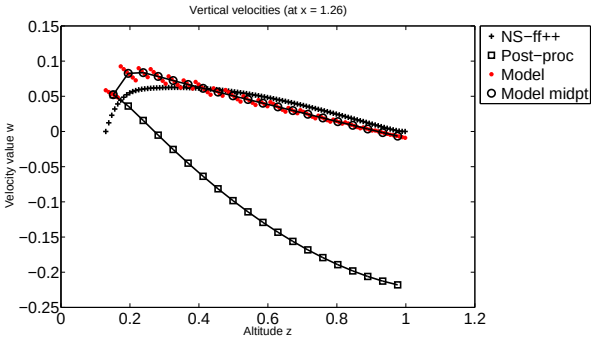

(c) Vertical Vel. $x = 1.26$

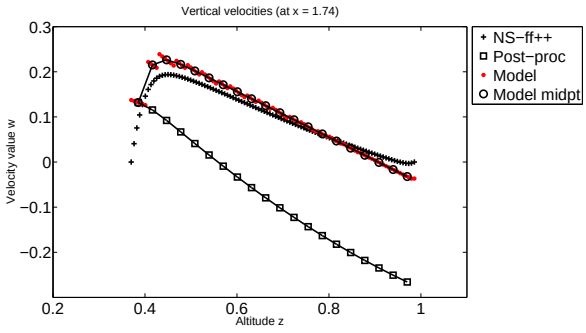

(d) Vertical Vel. $x = 1.74$

Figure 11: Horizontal and Vertical velocities at the positions $x = 1.26$ and $x = 1.74$ with viscosity $\nu = 10^{-3}\,\mathrm{m}^2 \cdot \mathrm{s}^{-1}$ and mean inflow $\bar{q} = 0.5\,\mathrm{m}^2 \cdot \mathrm{s}^{-1}$. $(N = 20)$.

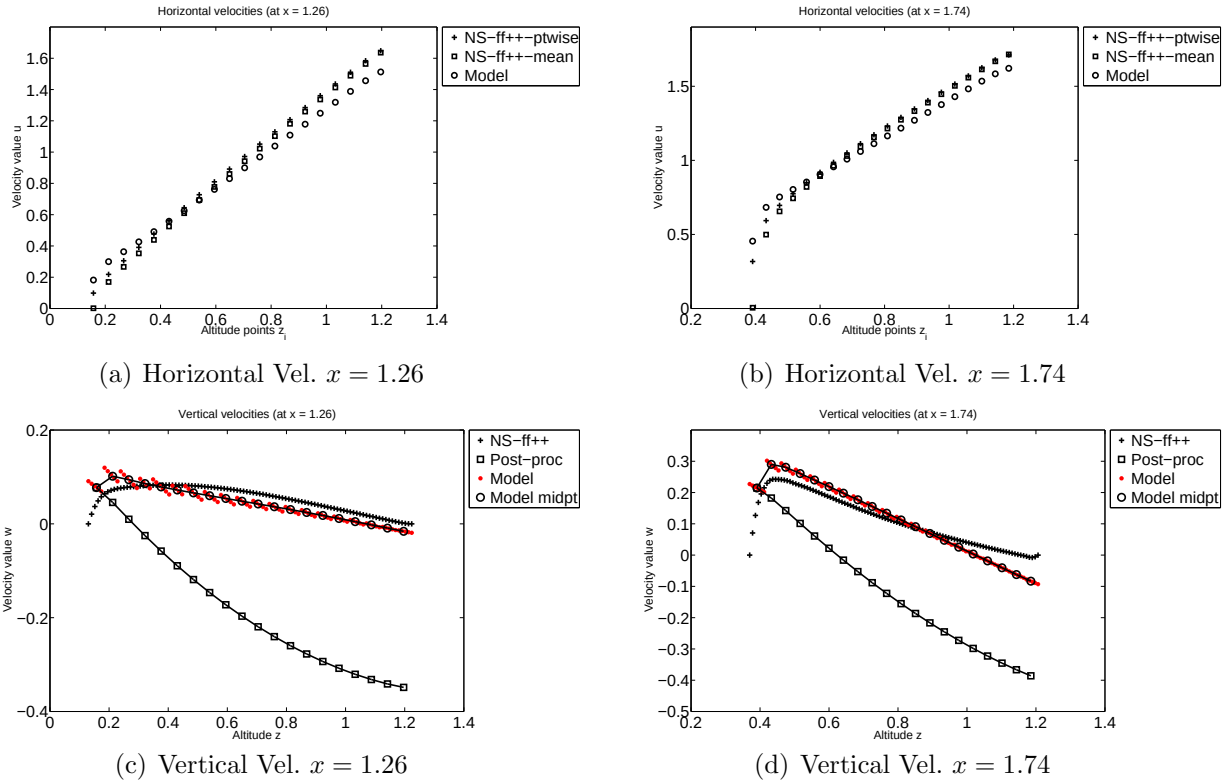

(a) Horizontal Vel. $x = 1.26$

(b) Horizontal Vel. $x = 1.74$

(c) Vertical Vel. $x = 1.26$

(d) Vertical Vel. $x = 1.74$

Figure 12: Horizontal and Vertical velocities at the positions $x = 1.26$ and $x = 1.74$ with viscosity $\nu = 10^{-3}\,\mathrm{m}^2 \cdot \mathrm{s}^{-1}$ and mean inflow $\bar{q} = 1\,\mathrm{m}^2 \cdot \mathrm{s}^{-1}$. $(N = 20)$.

6 Conclusion

In this work, we derive a multilayer system considering hydrostatic pressure. The governing equations of the system are similar to the one exhibited and analyzed in [8], assuming hydrostatic pressure too and using therein an asymptotic development technique. However the source terms, namely the momentum transmission through the artificial interfaces, and the vertical velocities are handled in a quite different way. Also the leading velocities at those interfaces are taken into account in different ways. Actually, we use here a particular approximation of the weak formulation of Navier-Stokes equations. This approximation consists in piecewise constant horizontal velocity and piecewise linear vertical velocity in the vertical direction. Moreover, from the normal flux jump conditions, involved by the weak formulation, we clarify the normal and tangential components of the stress at the interfaces. In the numerical test section we have shown that it can exist a large difference between the vertical component of the velocity when it is approximated by a simple post-procesing of the incompressibility condition or with the algorithm proposed in this paper. Finally, in the numerical test section we have shown, for a simple test, that the multilayer model produces accurate results in comparison with the approximation computed by a standard finite element method applied to the full NS equations.

Acknowledgements

We thank E. Audusse, M.J. Castro, A. Mangeney, J. Sainte-Marie and C. Parés for the interesting discussion on the multilayer approach during the conference "Numerical methods for Hyperbolic Equations Theory and Applications" to honour Professor E.F. Toro in his 65th birthday, in July 2011, Santiago de Compostela, Spain. We also thank the organizers of this conference to bring us this meaningful opportunity of meeting and discussion.

This work has been partially suported by Spanish Ministerio de Educación y Ciencia Research Project MTM2009-07719.

References

[1] C. Acary-Robert, E. Fernández-Nieto, G. Narbona-Reina, and P. Vigneaux. A well-balanced finite volume-augmented lagrangian method for an integrated herschel-bulkley model. *Journal of Scientific Computing*, 53:608–641, 2012.

[2] M. Amara, D. Capatina, and D. Trujillo. Variational approach for the multiscale modeling of an estuarian river. part1: Derivation and numerical approximation of a 2d horizontal model. *Report, INRIA*, RR-6742, 2008.

[3] E. Audusse. A multilayer Saint-Venant model: derivation and numerical validation. *Discrete Contin. Dyn. Syst. Ser. B*, 5(2):189–214, 2005.

[4] E. Audusse and M.-O. Bristeau. A well-balanced positivity preserving "second-order" scheme for shallow water flows on unstructured meshes. *J. Comput. Phys.*, 206(1):311–333, 2005.

[5] E. Audusse and M.-O. Bristeau. Finite-volume solvers for a multilayer Saint-Venant system. *Int. J. Appl. Math. Comput. Sci.*, 17(3):311–319, 2007.

[6] E. Audusse, M.-O. Bristeau, and A. Decoene. Numerical simulations of 3D free surface flows by a multilayer Saint-Venant model. *Internat. J. Numer. Methods Fluids*, 56(3):331–350, 2008.

[7] E. Audusse, M.-O. Bristeau, M. Pelanti, and J. Sainte-Marie. Approximation of the hydrostatic Navier-Stokes system for density stratified flows by a multilayer model: kinetic interpretation and numerical solution. *J. Comput. Phys.*, 230(9):3453–3478, 2011.

[8] E. Audusse, M.-O. Bristeau, B. Perthame, and J. Sainte-Marie. A multilayer Saint-Venant system with mass exchanges for shallow water flows. Derivation and numerical validation. *ESAIM Math. Model. Numer. Anal.*, 45(1):169–200, 2011.

[9] M. J. Castro Díaz and E. D. Fernández-Nieto. A class of computationally fast first order finite volume solvers: Pvm methods. *SIAM J. Sci. Comput.*, 34(4):2173–2196, 2012.

[10] T. Chacón Rebollo, A. Domínguez Delgado, and E. D. Fernández Nieto. An entropy-correction free solver for non-homogeneous shallow water equations. *M2AN Math. Model. Numer. Anal.*, 37(5):755–772, 2003.

[11] G. Dal Maso, P. G. Lefloch, and F. Murat. Definition and weak stability of nonconservative products. *J. Math. Pures Appl. (9)*, 74(6):483–548, 1995.

[12] E. Fernández-Nieto, E. Koné, T. Morales, and R. Bürger. A multilayer shallow water system for polydisperse sedimentation. *J. Comp. Physics (to appear)*, 2013.

[13] E. D. Fernández-Nieto and G. Narbona-Reina. Extension of WAF type methods to non-homogeneous shallow water equations with pollutant. *J. Sci. Comput.*, 36(2):193–217, 2008.

[14] H. Frédéric. Freefem++ home page. *http://www.freefem.org/ff++/*, 2012.

[15] C. Parés. Numerical methods for nonconservative hyperbolic systems: a theoretical framework. *SIAM J. Numer. Anal.*, 44(1):300–321 (electronic), 2006.

[16] C. Parés and M. Castro. On the well-balance property of Roe's method for non-conservative hyperbolic systems. Applications to shallow-water systems. *M2AN Math. Model. Numer. Anal.*, 38(5):821–852, 2004.

[17] J. Sainte-Marie. Vertically averaged models for the free surface non-hydrostatic Euler system: derivation and kinetic interpretation. *Math. Models Methods Appl. Sci.*, 21(3):459–490, 2011.

[18] I. Toumi. A weak formulation of Roe's approximate Riemann solver. *J. Comput. Phys.*, 102(2):360–373, 1992.

[19] J. Yan and C.-W. Shu. A local discontinuous galekin method for kdv type equations. *Siam J. Numer. Anal.*, 40(2):769–791, 2002.